1   **Combining colour parameters and geochemical tracers to improve sediment source discrimination**

2   **in a mining catchment (New Caledonia, South Pacific Islands)**

3   Virginie Sellier[1] • Oldrich Navratil[2] • John Patrick Laceby[3] • Cédric Legout[4] • Michel Allenbach[5] • Irène

4   Lefèvre[1] • Olivier Evrard[1]

5   [1]Laboratoire des Sciences du Climat et de l'Environnement (LSCE), UMR 8212 (CEA/CNRS/UVSQ-IPSL),

6   Université Paris-Saclay, Gif-sur-Yvette (France)

7   [2] Laboratoire Environnement Ville Société (EVS), Université Lumière Lyon 2, UMR 5600 (CNRS), Lyon

8   (France)

9   [3] Alberta Environment and Parks, Calgary, Alberta (Canada)

10   [4]Institut des Géosciences de l'Environnement (IGE), UMR 5001, Grenoble (France)

11   [5]LIVE-EA 4243, Université de Nouvelle-Calédonie & LABEX Corail, Nouméa (Nouvelle-Calédonie,

12   France)

13   **Corresponding author:** selliervirg@free.fr ; Tel: (33)673910072

Abstract

15   Over the last century, the intensification of metal mining practices has induced significant land-

16   cover changes that have accelerated soil erosion processes in mining countries. In New Caledonia, a

17   French archipelago located in the south-west Pacific Ocean, open-cast nickel mining is responsible for

18   soil degradation in almost 10 % of the archipelago's area. This soil degradation results in particular in

19   the increased downstream transfer of sediments in river systems, leading to concerns of siltation of

20   the river systems. In order to reduce this sediment input, quantifying the sediment source

21   contributions from mining activities is required to effectively target the management measures to

22   implement (e.g. types of engineering works, sizing). Spectroscopy which is a rapid, inexpensive and

23   non-destructive alternative technique to the analysis of geochemical fingerprinting properties may be

24   used to investigate whether eroded sediment is derived from mining sub-catchments or non-mining

25   sub-catchments. Sediment deposited during two cyclonic events (i.e. 2015 and 2017) was collected

26   following a tributary design approach in one of the first areas exploited for nickel mining, the Thio River

27   catchment (397 km²). Source (n= 24) and river sediment (n= 19) samples were analyzed by X-ray

28   fluorescence and spectroscopy in the visible spectra (i.e. 365-735 nm). Four fingerprinting approaches

29   based on (1) colour parameters, (2) geochemical properties, (3) colour parameters coupled with

30   geochemical properties and (4) the entire visible spectrum were tested to discriminate and estimate

31   sediment source contributions.

32   The results demonstrated that the individual sediment tracing methods based on spectroscopy

33   measurements (i.e. (1) and (4)) did not provide sufficient discrimination between sources. However,

34   the inclusion of colour properties in addition to geochemical parameters (3) provided the highest

35   discrimination between sources (i.e. 92.6 % of source variance explained). Although with a slightly

36   lower discrimination potential (i.e. 83.1 % of variance explained in sources), the geochemical approach

37   (2) provided similar results to those obtained with the colour coupled with geochemical approach (3).

38   For each of these approaches (2) and (3), the associated fingerprinting properties were used in an

39   optimized mixing model. The predictive performance of the models was validated through tests with

40   artificial mixture samples, i.e. where the proportions of the sources were known beforehand. The

41   results obtained with model (3) showed that mining tributary contributions strongly dominated the

42   sediments inputs with a mean contribution of 68 ± 25% for the 2015 flood event and 88 ± 8% for the

43   2017 flood event. Therefore, the use of these approaches based on geochemical properties individually

44   (2) and coupled to colour parameters (3) could be extended to other mining catchments of New

45   Caledonia but also to other similar nickel mining catchments around the world to estimate sediment

46   source apportionment.

48   **Keywords:** Nickel mining • Sediment source fingerprinting • Soil erosion • Modeling

1.Introduction

At the dawn of a fourth industrial revolution, demand for metalliferous minerals continues to increase and impact the world market (Prior et al., 2013;Highley et al., 2004). Currently, open-cast mining generates more than three-quarters of the world's metal ores. However, the extraction of these minerals is associated with deleterious impacts on the environment. In particular, these mines are responsible for the increase in soil erosion and the accelerated transfer of sediment in the river systems. Indeed, bare soil areas generated by mining activities including exploitation sites, prospection areas and access roads significantly increase runoff production (Yellishetty et al., 2013;Dumas et al., 2010;Abel et al., 2000). Moreover, the extraction of mineral ore is accompanied by a sharp production of mining wastes. Until the 1980s, no environmental regulation had been implemented to store this mining waste, and it was dumped directly onto the mountain slopes (Valette-Silver, 1993). Currently, this legacy mining waste provides an active source of sediment as it can progressively be remobilized (Coulthard and Macklin, 2003;James, 2013).

New Caledonia, an island located in the south-western Pacific Ocean and currently the world's sixth-largest producer of nickel, is in particular challenged with the problems of siltation of its river systems. Several studies outline how mining activities, which started in 1875, are generally responsible for these river morphological changes (Bird et al., 1984;Iltis, 1992;Garcin et al., 2017). In this case, excessive inputs of fine and coarse sediment triggered mainly during extreme rainfall events (e.g. cyclones and tropical depressions) have led to the disturbance of the sediment cascade in the river systems. A raising and widening of the riverbed has in particular been observed in the New Caledonian river systems by Garcin et al. (2017), leading to the increased occurrence of flooding events in these tropical regions. Owing to the occurrence of major cyclones in New Caledonia (i.e. on average one cyclone every 2.7 years (Garcin, 2010)), the local population regularly has to deal with the damage generated by these flood events: damage to human settlements, public infrastructure, agricultural land and human casualties. Moreover, suspended sediment is known to transport large quantities of contaminants in

75 river systems (Kumar and Maiti, 2015;Priadi et al., 2011;Varol, 2011). Hedouin et al. (2007), and more

76 recently Baudrimont et al. (2019), observed high concentrations of trace metals, including Ni and Cr,

77 in marine and freshwater organisms in New Caledonia. These observations raise many questions about

78 the health impact of mining activities on the populations who eat a lot of fish. On a more global level,

79 this anthropogenic activity also threatens the second largest coral reef in the world, listed as a UNESCO

80 World Heritage (Davis and Fox, 2009). In particular, the increased turbidity associated with sediment

81 supply could disrupt coral metabolism (i.e. photosynthetic processes) (Juillot, 2019). These coral reefs

82 provide an exceptional biological diversity and deliver several essential ecosystem services to the local

83 population including fisheries, coastal protection and tourism (Pascal, 2010). The implementation of

84 effective and long-term sediment control measures on mining sites (e.g. sediment retention basin,

85 revegetation) is therefore required to reduce sediment inputs into the lagoon. At this end, quantifying

86 the sediment source contributions from mining activities becomes particularly important as the mining

87 industries are subject to the "polluter pays" principle applied since 1975, i.e. the obligation to fund

88 remediation according to the extent of the damage generated by mining activity on the environment

89 (Clarke and David, 2010). Discriminating between sediment sources generated by mining activities and

90 other potential sediment sources is therefore a real social, environmental, political and financial

91 challenge in New Caledonia.

92 Indeed, other sediment sources that are not associated with mining activities as deforestation,

93 farming, pasture may contribute to sediment inputs in river systems. The use of fires to clear

94 landscapes also increases the area of bare soils (Dumas et al., 2010). Moreover, several invasive species

95 such as deers or wild pigs threaten soil stability through trampling and overgrazing (Shellberg et al.,

96 2010). Soils that are left uncovered with vegetation are more sensitive to erosion and they may be

97 exposed to landslides (Blake et al., 2009;Smith et al., 2011).

98 Sediment fingerprinting techniques have been developed since the 1970s to determine the

99 spatial origin of sediment sources and quantify their contributions (Klages and Hsieh, 1975;Walling et

al., 1979;Brown, 1985). These techniques are based on the analysis of multiple conservative properties both in the sediments and their potential sources. The properties must necessarily be conservative, i.e. the ranges of variation of these properties in the river material have to be predictable based on those measured in the sediment sources. The ability of one or more of these properties to discriminate between sources then allows to estimate the relative contribution of each source through the use of a mixing model (Collins and Walling, 2002). Fallout radionuclides (Wallbrink, 2004;Evrard et al., 2015;Evrard et al., 2020), geochemical (Laceby and Olley, 2015;Batista et al., 2018) and mineral properties (Gruszowski et al., 2003;Motha et al., 2004) are the most frequently used tracers to quantify sediment source contributions. The use of fallout radionuclides and geochemical properties as potential tracers was investigated to quantify the sources of suspended sediment in the Thio River catchment (397 km²), one of the first catchments in New Caledonia to be mined for nickel. Fallout radionuclides proved to be unsuitable (i.e. non-discriminatory) while geochemical properties provided promising results, i.e. 83.1 % of variance explained in sources (Sellier et al., 2019). The discrimination offered by geochemical properties was particularly explained by the differences in geochemical composition outlined by Sevin (2014) between the two dominant lithologies found in the archipelago: volcano-sedimentary formations covering two thirds of the archipelago and peridotite massifs covering the remaining third where mining activities are located. Mining erosion dominates 95% of eroded areas identified on peridotite massifs of the Thio River catchment according to the remote sensing study carried out by Garcin et al. (2017). As a result, using geochemical properties is effective to indirectly quantify the sediment contributions from mining activities and from areas devoid of mining activities. In this case, K provides a straightforward tracer to discriminate the sediment sources (Sellier et al., 2019). Indeed, volcano-sedimentary rock formations naturally contain high K elemental contents whereas peridotite massifs are depleted in this element in New Caledonia (Sevin, 2014). Although these initial study results were very promising, other less expensive, faster and possibly more efficient techniques than the more conventional methods previously tested could be envisaged. For example, spectroscopy in the mid-infrared (MIR) (Poulenard et al., 2009), the visible near-infrared

126 (VNIR) and the shortwave-infrared (SWIR) (Brosinsky et al., 2014) spectra have been used to quantify

127 the sediment source contributions. Spectroscopy is also non-destructive and requires low quantities

128 of sample material. Spectroscopy could therefore meet both the need for a simple, inexpensive, fast

129 and portable sediment tracing method in a context where flood events are frequent. This analysis

130 technique could also be more easily transferred to local populations so that they can carry out long-

131 term environmental monitoring of sedimentary contributions themselves.

132 Moreover, the geological specificity of the archipelago provides a strong contrast in terms of soil

133 colours observed either on the peridotite massifs or on the volcano-sedimentary formation rocks and

134 by extension, on the eroded sediments derived from these soils. On the one hand, the weathering of

135 peridotite massifs naturally enriched in Fe and transition metals such as Mn, Ni, Cr and Co results in

136 the formation of laterite profile composed of peridotites, saprolites, yellow laterites and red laterites

137 (from the bottom to the top). Hypermagnesian and ferrallitic ferritic soils that are rich in goethite and

138 hematite and that formed on the surface provide a particularly reddish-orange colour to sediment

139 derived from these exploited soils (i.e. mining sources, Figure 1) (Quantin et al., 1997;Trescases, 1973).

140 On the other hand, the weathering of volcano-sedimentary formation rocks generates the formation

141 of altered horizons rich in goethite and clay horizons rich in kaolinite (from the bottom to the top)

142 (Denis, 1988). The eroded sediment derived from fersialitic soils formed on the surface is characterized

143 by a yellow-grey colour (Figure 1). The differences made visually between the two sources further

144 encourage the analysis of sources by spectroscopy and especially spectroscopy in the visible region of

145 the spectrum (i.e. 365-735 nm). In particular, the colorimetric parameters derived from the visible

146 spectrum have been shown to be effective in discriminating sediment sources. Their discrimination

147 power has been tested both individually (Evrard et al., 2019;Martínez-Carreras et al., 2010;Uber et al.,

148 2019) and in combination with other tracers (e.g. geochemical properties (Tiecher et al., 2015))

149 according to the conventional fingerprinting approach (i.e. statistical analysis and use of a mixing

150 model) (Collins et al., 1996). A more alternative approach based on the entire visible spectrum with

151 the partial least square regression (PLSR) models has also been developed to trace origin of sediment

152 sources in the literature (Legout et al., 2013;Tiecher et al., 2015).

153

154 **Figure 1** Photographs of river material deposited on the channel banks of a mining tributary (left) and a
155 non-mining tributary (right) in the Thio River catchment

156 As part of this study, four sediment fingerprinting methods based on (1) colour parameters, (2)

157 geochemical properties, (3) colour parameters coupled with geochemical properties and (4) PLSR

158 models based on the whole visible spectrum were tested in the Thio River catchment. A tributary

159 design approach was implemented to trace the origin of sediments, i.e. sediment samples collected on

160 different tributaries were used as potential sources of the river sediment collected further

161 downstream on the Thio River (Laceby et al., 2017). Source (n=24) and river sediment (n=19) samples

162 were collected and analyzed by X-ray fluorescence and spectroscopy in the visible spectra (i.e. 365-

163 735 nm). For each of these sediment fingerprinting methods, the associated potential tracing

164 properties were used in an optimized mixing model. Tests with artificial mixture samples, i.e. where

165 the proportions of the sources were known beforehand were carried out to evaluate the predictive

166 performance of each model in order to select the best technique to be applied in the Thio River

167 catchment and possibly in other mining catchments of New Caledonia.

2. Materials and methods

2.1 Study area

Located in the southwestern Pacific Ocean, New Caledonia (18 500 km²) is made up of several islands, the largest of which is *La Grande Terre* (17 000 km²). The Thio River catchment (397 km²) is located on the east coast of this island (Figure 2-a). It has a mountainous relief, with an average altitude of 416 m above sea level (i.e. minimum: 0 m, maximum: 1392 m, Figure 2-a) and an average slope of 45%. Two dominant lithologies are present in the catchment: volcano-sedimentary formations mainly located on the western part of the catchment and peridotite massifs concentrated in the eastern part of the catchment. Cherts (22 %), sandstone (9 %), a mix of basalt, dolerite and gabbro (6 %), polymetamorphic rocks (6 %) mainly constitute volcano-sedimentary formations whereas peridotite massifs are composed of laterites (18 %), peridotites (17 %), serpentines (10 %) and hazburgites (1 %) (Garcin et al., 2017) (Figure 1-b). The rock formation of these lithologies plays a key role in determining their degree of soil erodibility. In this case, Dumas (2010) described that volcano-sedimentary formations are less sensitive to soil erosion than peridotite massifs. Indeed, rocks from volcano-sedimentary formations such as basalts and cherts provide a certain resistance to erosion whereas laterites at the top of the profile are extremely sensitive to erosion processes, which explains why most forms of concentrated erosion (e.g. gullies, rills) and mass movements are mainly observed on peridotite massifs (Figure 3). However, the permanent vegetation covering 96% of the Thio River catchment surface offers a relative protection against soil erosion across the catchment. Peridotite massifs naturally enriched in heavy metals have a low soil fertility, which explains why farming or pasture activities are not implemented on these soils (Quantin et al., 1997). Peridotite massifs have been exploited exclusively for their nickel resources since 1875. According to the mining registry, active and abandoned mining sites and exploration cover 21 % of the catchment area (Figure 2-c).

192   The Thio River catchment is subject to a tropical climate characterized by the alternation of a

193   hot wet season (November-April; mean temperature of 27 °C) and a cooler dry season (May-October;

194   mean temperature of 20 °C). The mean annual rainfall in the Thio River catchment is 1620 mm despite

195   strong seasonal fluctuations with the highest levels of precipitation recorded during the cyclonic

196   season between January and March (700 mm, 1981-2008; Alric (2009)). Although they only occur on

197   average once every 2.7 years, cyclones or tropical depressions may supply more than 20 % of the

198   annual rainfall in only one day according to local meteorological records (Météo France).

199

200   Twelve major tributaries flow into the main stem of the Thio River (28 km long) (Figure 2-b).

201   Ninety-two percent of the river channel length are characterized with slopes lower than 5 %. According

202   to Surell's classification (1841), the Thio River can be considered as torrential except in its estuarine

203   section. In addition, the longitudinal connectivity is exacerbated by the 8km² of bare soils associated

204   with past mining activities (~10 sites), ongoing mining operations (e.g. 2 sites: Thio Plateau, Camps des

205   Sapins) and the occurrence of 6 km² of mining roads. Bare soil areas increase soil erosion processes on

206   peridotites massifs, which once initiated, are difficult to contain (Figure3). Heavy rainfall and the

207   associated runoff exacerbate the widespread occurrence of rills, gullies, landslides (Danloux and

208   Laganier, 1991), thus contributing to connect the sediment sources to the tributaries and consequently

209   to the main river (Figure 3). For low intensity floods (i.e. <200 $m^3.s^{-1}$), a strong remobilization of

210   sediments in New Caledonian river systems has been observed (Allenbach et al., 2020), thereby

211   indicating that a lateral connectivity occurs in the Thio River catchment through the occurrence of

212   channel bank erosion.

213

214

a.

215

b.

c.
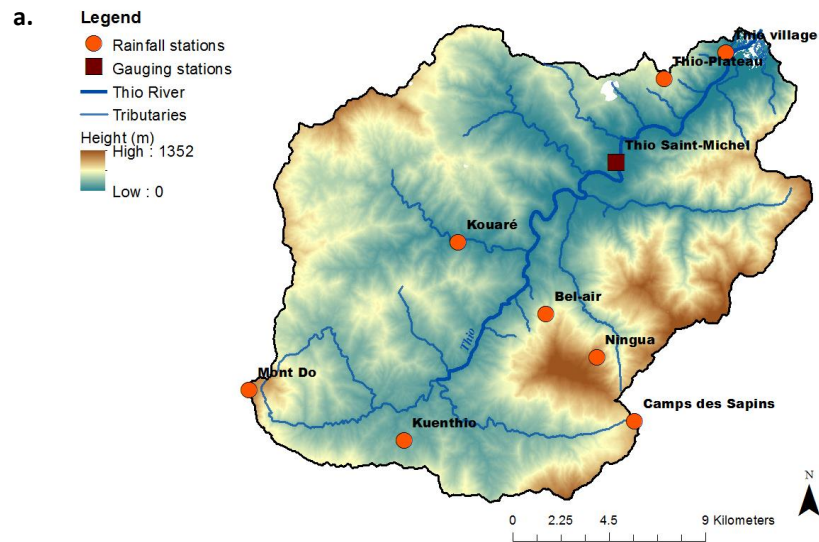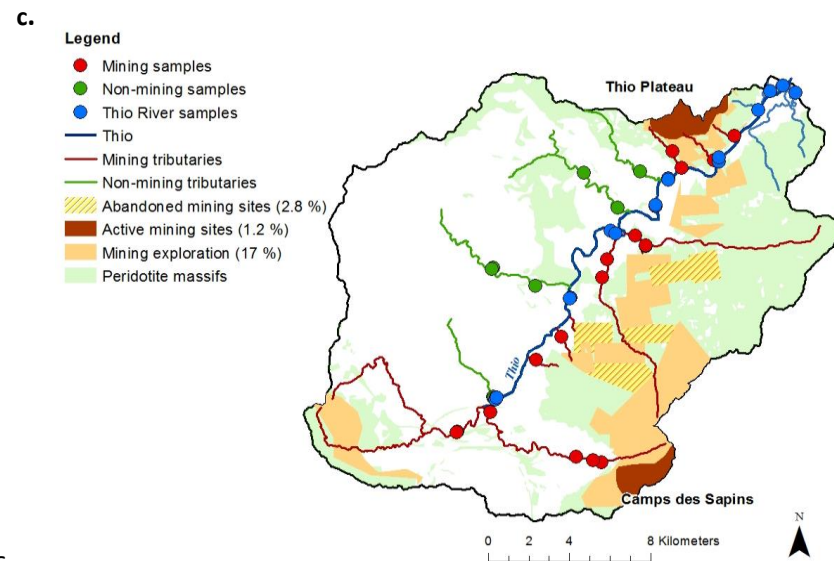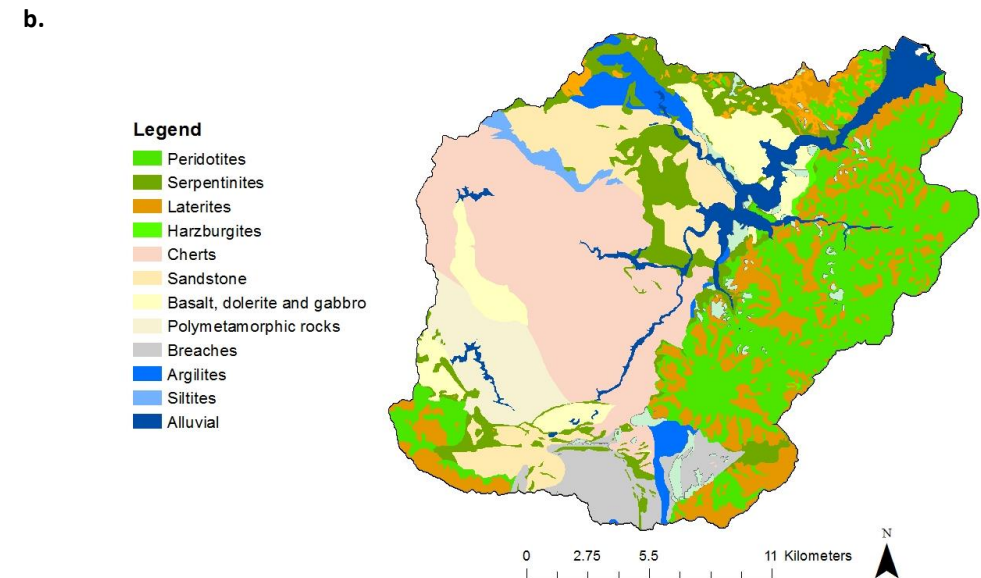
216

Figure 2 Location of the rainfall and river monitoring stations (a), main lithologies (b) and location of the sediment samples collected along with tributary source classifications (c) conducted in the Thio River catchment, New Caledonia

217

218

219 **Figure 3** Photographs of concentrated erosion and mass movement processes observed on peridotite
220   massifs of the Thio River catchment

221   **2.2 Hydro-sedimentary monitoring**

222   Three rainfall stations (Thio Plateau, Thio village, Camps des Sapins; Figure 2-b) are operated by

223   Météo France and five others are managed by the DAVAR (Direction des Affaires Vétérinaires

224   Alimentaires et Rurales; i.e. Kouaré, Bel-Air, Ningua, Kuenthio, Mont Do), with daily records available

225   since 1952 for some stations (e.g. Thio village). Daily discharge has been monitored at a river gauging

226   station located on the main stem of the Thio River (at Saint-Michel) since 1981 by the DAVAR (Figure

227   1-a).

228   **2.3 Sources and river sediment sampling**

229   In this study, two extreme events were investigated: Cyclone Murcia on February 25, 2015 and

230   Cyclone Cook on April 10, 2017. These cyclones respectively contributed to 7 % of annual rainfall in

231   2015 and 25 % in 2017. They generated floods with a return period of 10 years (i.e. 3500 $m^3.s^{-1}$). To

232   trace the origin of sediment, lag deposits were collected as an alternative of suspended sediment

233   sampling on channel bars of mining tributaries (n= 16), non-mining tributaries (n= 8) and the Thio River

234   (n= 19) according to the tributary design approach recommended by Laceby et al. (2017) (Figure 2-c).

235   They were sampled after the two major floods generated by Cyclone Murcia (n= 31) and Cyclone Cook

236   (n= 12). These two sample sets were respectively sampled between April 30 and May 5, 2015 and

237   between May 16 and 17, 2017. At each sampling site, five to ten subsamples of fine sediment were

238   collected depending on the amount of observed sedimentary material. They were sampled across a 10

239   m² surface with a plastic trowel at exposed subaerial sites free of vegetation on channel bars. The

240   subsamples were composited into one sample representative of the fine sediment deposited on the

241   channel bars. The samples were oven-dried at 40°C for ~48 hours. Particle size selectivity may occur

242   during the erosion, transport and deposition processes inducing an overall finer particle size

243   distribution in the river material compared to the sources. This selectivity can lead to a non-

244   conservation of the fingerprinting properties. For example, certain properties are preferentially

245   contained in a given particle size fraction which can create a relative enrichment or conversely a

246   relative depletion of these properties in the river material according to the particle size fraction

247   analyzed. In order to avoid this particle size effect, river sediment and source samples were sieved to

248   63 μm, which is the most commonly used fraction in sediment tracing research (Owens and Walling,

249   2002;Navratil et al., 2012).

250   **2.4 Preparation of artificial mixture samples**

251   Equal quantities of all mining tributary samples (0.4g for each sample, n= 16) were mixed

252   together to create a composite sample which would have an overall geochemical and colour signature

253   of the mining sources in the Thio River catchment (i.e. 'Mining source' pole). The same process was

254   carried out with non-mining tributary samples(0.4g for each sample, n= 8, 'Non-mining source' pole).

255   'Mining source' and 'Non-mining source' pole samples were then mixed in known proportions to create

256   artificial mixture samples (n= 21, 0-100 % with a 5 % step, Table 1).

257

258 **Table 1** Proportions of mining and non-mining sources (%) in artificial mixture samples (M_i). *M6 was*

259 *withdrawn from this study because an error occurred at the time of its completion (not consider in the study).*

M_i	Proportions of 'mining source' pole (%)	Proportions of 'non-mining source' pole (%)
M1	0	100
M2	5	95
M3	10	90
M4	15	85
M5	20	80
M6	*25*	*75*
	(not consider in the study)	*(not consider in the study)*
M7	30	70
M8	35	65
M9	40	60
M10	45	55
M11	50	50
M12	55	45
M13	60	40
M14	65	35
M15	70	30
M16	75	25
M17	80	20
M18	85	15
M19	90	10
M20	95	5
M21	100	0

260

261 **2.5 Source, river sediment and artificial mixture sample analyses**

262 Spectroscopy measurement in the visible were carried out with a portable diffuse reflectance

263 spectrophotometer (Konica Minolta 2600d) at the Institut des Géosciences de l'Environnement (IGE,

264 Grenoble, France). To this end, between 0.1 g and 4 g of Thio River sediment (n= 19), source (n= 16)

265 and artificial mixture samples (n= 20) were stored in 60 mL polystyrene tubes. In order to perform the

266 analyses, the spectrophotometer was installed on a flat surface with the measuring window facing

267 upwards. The tubes were then placed on the 3-mm radius circle measuring cell. Because of the rather

268 small measuring area and to take into account the possible heterogeneity within the samples, three

269 measurements were carried out on river sediment and sources samples. For artificial mixture samples,

270 the experimenter who conducted the analyses performed four measurements. Spectral reflectances

271   were measured between 365 nm and 735 nm with a 10-nm resolution. Several parameters were

272   applied for each measurement: D65 illuminant, 10° angle observer and specular component excluded.

273   Raw data collected corresponds to the spectral reflectance percentage for each of the 39-wavelength

274   classes. From these raw data, 15 variables of various colorimetry models were derived. Among these

275   components, XYZ tri-stimulus values were calculated based on the colour-matching functions defined

276   by the International Commission on Illumination (CIE 1931). The standardized tri-stimuli were then

277   converted into CIELab and CIELu'v' cartesian coordinate systems using the equations provided by CIE

278   (1976) and then into CIELch, CIEL*a*b* cartesian coordinate systems using the equations provided by

279   CIE (1994) (Rossel et al., 2006). First Derivative reflectance of the Visible Spectra (FDVS) of each sample

280   was also derived from the initial reflectance spectrum. According to Tiecher et al. (2015), the use of

281   FDVS avoids differences in baseline positions and allows to get rid of the small differences due to

282   uncontrolled sources of variation, as sample packaging. A zero and a white calibration were performed

283   before each set of measurements. In addition, and in order to evaluate a potential drift of the device's

284   signal, control measurements were carried with red, green, yellow panels and three contrasted

285   sediment samples before and after each set of measurements.

286   Measurements of 11 geochemical elements *(*i.e. Mg, Al, Si , K, Ca, Ti, Cr, Mn, Fe, Ni and Zn) on

287   the samples were conducted by pre-calibrated energy dispersive X-ray fluorescence spectrometry

288   (Epsilon 3, Malvern PANalytical) with certified reference samples including Internal Atomic Energy

289   Agency (IAEA) standards. Correlations between the determined and the standard elemental contents

290   were comprised between 0.90 and 0.99. The associated mean relative error was 9 % (SD 8 %). Between

291   0.2 and 0.5 g of the samples were packed in small mass holder (SMH) cells with an air double X-ray

292   Mylar film and analyzed at the Laboratoire des Sciences du Climat et de l'Environnement (LSCE, Gif-

293   sur-Yvette, France). Samples were irradiated with a primary beam generated by an Rh anode X-ray

294   tube emitting electromagnetic waves between 100eV and 1MeV with a maximum power, typical

295   current and voltage fixed to 15 W, 3mA and 50 kV respetively. The associated Si-drift detector had a

296   Be window thickness of 8 µm and recorded the sample spectrum in a 2D optical geometry

297 configuration. X-ray intensities were converted into concentrations using the Epsilon 3 software

298 program through the application of the fundamental parameters method.

299 **2.6 Statistical analysis and sediment tracing**

300 2.6.1.Conventional mixing model

301 In general, the sediment source fingerprinting approach is composed of four main steps: (1)

302 range test, (2) the Mann-Whitney U test, (3) a stepwise discriminant function analysis and (4) a mixing

303 model (Collins et al., 1996;Laceby and Olley, 2015). For the range test, all variables exhibiting values in

304 the river sediment samples that were outside of the range found in the potential sources (i.e. between

305 the minimum and maximum values found in source samples) were excluded from the analysis. It is

306 important to restrict the tracing parameters to those that show a conservative behavior to avoid

307 incorrect source prediction and consequently inaccurate estimations of source contributions (Sherriff

308 et al., 2015). Thereafter, the Mann-Whitney U test (α= 0.05, p-value <0.01) was performed to evaluate

309 whether remaining variables could discriminate the source samples. A stepwise discriminant function

310 analysis (DFA) was independently run on three set of potential tracing properties: (1) colour

311 parameters (i.e. 'colour'), (2) geochemical properties (i.e. 'geochemistry') and (3) colour parameters

312 and geochemical properties (i.e. 'colour + geochemistry'). For the last set, the raw values of the

313 variables were normalized in order to make them comparable. Indeed, several colour parameters were

314 within an order of magnitude of around 0.01 whereas for the geochemical parameters the difference

315 was around 10^6 mg kg^{-1} which resulted in a poorly conditioned matrix for the DFA.

316 The following calculation was therefore applied on the variable values to normalize them: x_i –

317 x_{min}/ x_{max} - x_{min} where xi was value found in source sample (i), x_{min} and x_{max} were respectively the

318 minimum and maximum values found in the source samples. The DFA was carried out to select the

319 optimal number of potential tracers to discriminate the sources for each modelling approach with the

320 optimal number of potential tracers which must provide the lowest Wilks' lambda value from analysis

321   of variance. Indeed, the closer the Wilks' lambda value is to 1, the lower the variability within the

322   sources compared to the total variability. The DFA was performed in the backward mode with a p >0.01

323   used to select a tracer and p <0.01 used to remove a tracer. The *Statistica* software was used to carry

324   out the DFA because it has the advantage of automatically identifying and eliminating collinear

325   variables.

326   Finally, a classical solver-based mixing model was used to model the source contributions from

327   the mining and non-mining tributaries to target sediment through simultaneously minimizing the

328   mixing model difference (MMD) (Evrard et al., 2019):

329
$$MMD = \sum_{i=1}^{n}((C_i - (A_i x + B_i(1-x))/C_i) \quad Equation\ 1$$

330   where n is the number of parameters in the model chosen by the selection process (i.e. steps 1, 2, 3);

331   C_i is the Thio River sediment sample parameter (i); x and (1-x) were respectively the contributions of

332   source A and B (i.e. mining and non-mining tributaries); A_i is the mean of parameter (i) in source A and

333   B_i is the mean of parameter (i) in source B. The proportional contribution from each source (x) was

334   modelled by solving Equation 1 with the Solver Function in Microsoft Excel with x being between 0 and

335   1 and the sum of source contributions (i.e. x and 1-x) equaling 1. The GRG Non-Linear solving method

336   was used with automatic scaling in Solver, ignoring integer constraints, with a maximum run time of

337   5000 and allowing for 2500 iterations. For each of the 2500 iterations, the values of the variables were

338   determined randomly with respect to their initially fixed ranges of values. A constraint precision and

339   convergence of 1.0 10^{-6} were selected for each of the model runs. To test the reliability of the 'colour',

340   'geochemistry' and 'colour + geochemistry' models, these latter were tested on artificial mixture

341   samples.

342   2.6.2.FDVS- PLSR model

343   FDVS-PLSR models were built following the methodology described in Poulenard et al. (2012).

344   The first step consisted in applying a principal component analysis (PCA) to evaluate the overall

345   variability between FDVS (i.e. 38-wavelength class) of source samples. Subsequently, a discriminant

346   analysis (DA) was conducted based on the PCA scores. The purpose of this analysis was to compare the

347   Mahalanobis distance between sources samples and to determine if FDVS of source samples could

348   discriminate the sources. Relationships between FDVS (x variate) and the corresponding weight

349   contribution of the sediment source data sets (y variate) were analyzed using PLSR. The PLSR models

350   were carried out based on the component set providing the lowest predictive error (PRESS, option on

351   XLStat software). Two independent PLSR models were built to estimate the two sediment source

352   contributions. As the artificial mixtures were measured four times by spectroscopy, 84 FDVS of artificial

353   mixture samples were generated including 50 values that were randomly selected to build the models

354   (training set (ST)) and 34 to validate the models (validation set (SV)). The SV:ST ratio used was

355   approximately 1:2, which is in agreement with recommendations provided in the literature

356   (Daszykowski et al., 2002). To evaluate the performance of PLSR models, several indicators such as

357   coefficient of linear regression (r^2), root mean square error of calibration (RMSEC) and root mean

358   square error of prediction (RMSEP) values were calculated. Unlike the conventional fingerprinting

359   approach, the estimated contributions of sources were not limited to be in the range of 0 % and 100

360   %. In a similar way, the sum of source contributions was not constrained to be equal to 100 %. As a

361   result, another way to control the reliability of predictions was to sum the prediction proportions of

362   both models (Legout et al., 2013). FDVS of river sediment samples were then introduced into these

363   PLSR models to estimate the contribution of sediment sources.

364   **3.Results**

365   **3.1 Source description**

366   The ranges of values of all colour parameters measured in the Thio River sediment samples

367   systematically plotted within the range of values observed in the two potential sources (i.e. mining and

368   non-mining tributaries; Figure 4 and Table 2). The range test results confirmed the conservative

369   character of these parameters. For geochemical properties, elemental concentrations measured in the

370   river sediment also plotted within the range of concentrations found in sources (Sellier et al., 2019). In

371   similar way, the range tests applied on geochemical properties showed that all these properties were

372   also conservative.

373
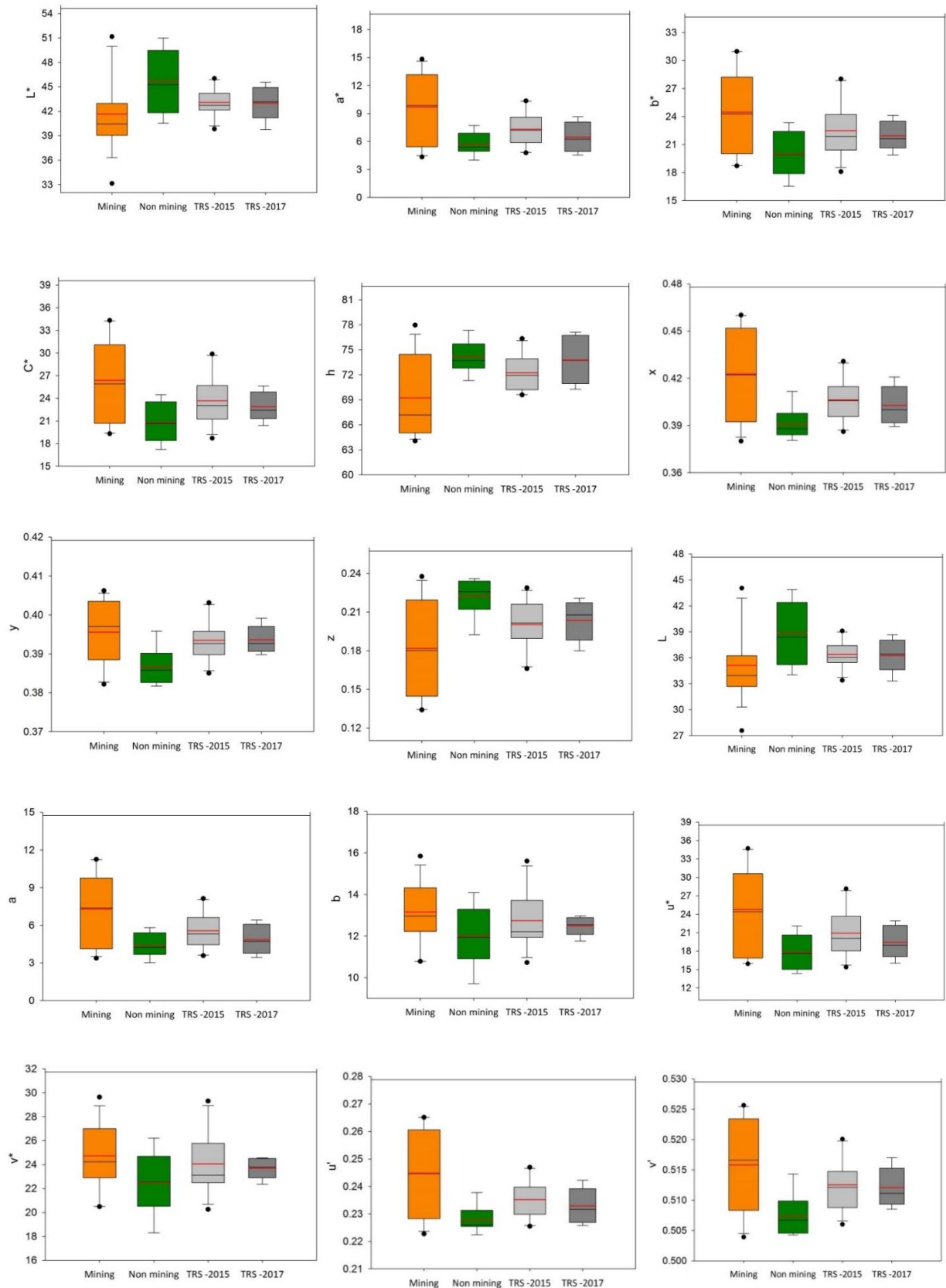
Figure 4 Box-plots of colour parameter values in the <63 µm fraction of sediment collected on the mining tributaries (Mining), non-mining tributaries (Non-mining) and the main Thio River (Thio River sediment (TRS)-flood events of 2015 and 2017). The box indicates the location of the first and third quartiles; the black line indicates the median value; the red line indicates the mean value

378 **Table 2** Mean values of geochemical element contents and colour parameters in the <63 µm fraction of sediment
379 sources and Thio River sediment (SD: standard deviation); results of Mann-Whitney U test and individual DA used
380 to identify the potential tracers to differentiate sources supplying sediment to the Thio River

Fingerprinting property	Mann-Whitney U test		DA- correctly classified samples (%)	Mean ± SD			
	U-value	p-value		Mining tributaries (n= 16)	Non-mining tributaries (n= 8)	Thio River sediment 2015 (n= 11)	Thio River sediment 2017 (n= 8)
Geochemical tracers							
Al *(g kg⁻¹)*	8	0.000	87.5	21 ± 21	67 ± 8	43 ± 15	29 ± 6
Ca *(mg kg⁻¹)*	21	0.007	62.5	3731 ± 470	9286 ± 5194	5281 ± 1201	3945 ± 666
Cr *(mg kg⁻¹)*	124	< 0.0001	83.3	7480 ± 4606	706 ± 967	4359 ± 2185	5715 ± 1786
Fe *(g kg⁻¹)*	121	0.000	91.6	144 ± 70	62 ± 24	43 ± 15	29 ± 6
K *(mg kg⁻¹)*	2	< 0.0001	95.8	1657 ± 2160	14019 ± 3702	5944 ± 3294	3750 ± 974
Mg *(g kg⁻¹)*	119	0.000	83.3	99 ± 59	16 ±13	88 ± 33	117 ± 21
Mn *(mg kg⁻¹)*	108	0.006	83.3	2531 ± 1317	1439 ± 606	2068 ± 667	1786 ± 516
Ni *(mg kg⁻¹)*	125	< 0.0001	91.6	6576 ± 5075	358 ± 339	4218 ± 1938	4341 ± 1239
Si *(g kg⁻¹)*	6	< 0.0001	91.6	178 ± 42	254 ± 28	221 ± 15	204 ± 7
Ti *(mg kg⁻¹)*	13	0.001	87.5	1409 ± 2077	5446 ± 835	2771 ± 1197	1663 ± 457
Zn *(mg kg⁻¹)*	68	0.834	-	146 ± 47	125 ± 4	134 ± 17	125 ± 8
Colour parameters							
L*	24	0.013	-	41.6 ± 4.6	45.7 ± 3.9	43.1 ± 1.7	43.0 ± 2.0
a*	104	0.013	-	9.7 ± 3.8	5.7 ± 1.2	7.3 ± 1.9	6.5 ± 1.7
b*	106	0.009	70.8	24.5 ± 4.5	20.0 ± 2.5	22.5 ± 3.0	21.9 ± 1.6
C*	108	0.006	66.6	26.4 ± 5.5	20.8 ± 2.7	23.7 ± 3.5	22.9 ± 2.0
h	26	0.019	-	69.2 ± 4.8	74.2 ± 1.9	72.2 ± 2.2	73.8 ± 2.9
x	107	0.007	75	0.42 ± 0.03	0.39 ± 0.01	0.41 ± 0.01	0.40 ± 0.01
y	111	0.003	79.2	0.396 ± 0.008	0.387 ± 0.005	0.393 ± 0.005	0.394 ± 0.004
z	19	0.005	75	0.18 ± 0.04	0.22 ± 0.01	0.20 ± 0.02	0.20 ± 0.02
L	27	0.013	-	35.1 ± 4.2	38.9 ± 3.7	36.4 ± 1.6	36.3 ± 1.9
a	103	0.016	-	7.3 ± 2.9	4.4 ± 1.0	5.6 ± 1.5	4.9 ± 1.2
b	91	0.106	-	13.1 ± 1.5	12.0 ± 1.5	12.7 ± 1.4	12.5 ± 0.4
u*	101	0.023	-	24.8 ± 6.9	17.8 ± 2.8	20.9 ± 4.0	19.4 ± 2.7
v*	93	0.081	-	24.7 ± 2.8	22.5 ± 2.7	24.1 ± 2.6	23.7 ± 0.8
u′	105	0.011	-	0.245 ± 0.016	0.228± 0.005	0.235 ± 0.007	0.233 ± 0.007
v′	111	0.003	79.2	0.516 ± 0.008	0.507 ± 0.004	0.513 ± 0.004	0.512 ± 0.003

381

3.2 Selection of parameters/properties for modelling

382

383   1.2.1. 'Colour' model

384   According to the Mann-Whitney U test results, six colour parameters (*i.e.* b*, C*, x, y, z, v')

385 provided significant discrimination between the two sediment sources (*i.e.* p-value < 0.01, Table 2).

386 The backward DFA selected only v' as the optimal tracer of mining and non-mining source sediments

387 (Figure 4, Table 3). Although this parameter correctly classified 79.2 % of sources, the high Wilk's

388 lambda value obtained (i.e. 0.7209, Table 3) induced that only 27.9 % of variance was explained by v'.

389 The low Mahalanobis distance value obtained (i.e. 1.6) confirmed that sediment sources were not well

390 separated. Accordingly, and owing to the high error percentage of the source discrimination provided

391 by this approach (i.e. 72.1 %), source contributions were not modeled with the 'colour' model.

392   1.2.2. 'Geochemistry' model

393   When considering the two potential sediment sources, all geochemical properties (except Zn)

394 were selected as potentially discriminant by the Mann-Whitney U test (i.e. p-value < 0.01, Table 2).

395 Among the 10 potential tracers, K was selected by the backward DFA to model sediment source

396 contributions from mining and non-mining tributaries with 95.3 % of sources correctly classified and

397 83.1 % of variance explained by K. This percentage of variance explained was deduced from the final

398 Wilk's lambda value obtained (i.e. 0.1691). Moreover, the Mahalanobis distance value showed that

399 the sediment sources were well separated from each other with a significant distance of 20.3 (Table 3)

400 (Sellier et al., 2019).

401   1.2.3. 'Colour + geochemistry' model

402   When combining colour parameters and geochemical properties, the DFA selected five optimal

403 tracers (i.e. K, Ca, Ti, b*, C*) able to correctly classify 100 % of the sources. A significant improvement

404 in the source discrimination was observed with the lowest Wilk's lambda value obtained (i.e. 0.0734)

405 and the highest percentage of variance explained (i.e. 92.6 %). Moreover, the Mahalanobis distance

406 value obtained (i.e. 52.1) was more than 2.5 times higher than that estimated with the 'geochemistry'

407 model (Table 3), thus resulting in a better separation between sediment sources than the previous

408 approach (i.e. 'geochemistry')

409 **Table 3** Results of DFA used to identify the optimum tracer combination to differentiate sources supplying
410 sediment to the Thio River

Fingerprint property selected	Wilks'Lambda	Variance explained by the variables (%)	Squared Mahalanobis distance	Correctly classified samples (%)
'Colour'				
v'	0.7209	27.9	1.6	79.2
'Geochemistry'				
K	0.1691	83.1	20.3	95.3
'Colour + Geochemistry'				
K, Ca, Ti, b*, C*	0.0734	92.6	52.1	100

411

3.3 Assessment of model performance on artificial mixture samples

413 Prior to applying mixing models to river sediments, preliminary tests were conducted to control

414 the validity of the models (i.e. 'geochemistry' and 'colour + geochemistry') and the associated

415 estimations of source contribution errors. When applying these models on the artificial mixture

416 samples, actual and predicted proportions were well correlated for both models (i.e. r^2= 0.99 and r^2=

417 0.98 respectively for 'geochemistry' and 'colour + geochemistry' models, SD_{max} = 3 %) (Figure 5).

418 However, the 'geochemistry' model described in Figure 5-a showed that the contributions of

419 mining tributaries were overestimated. With 100 % of actual mining contributions, 100 % of mining

420 contribution was predicted by the model. However, instead of 0 % of actual mining contributions, a

421 mining contribution of 15.5% was predicted by the model. It means that the more the estimated

422 mining source contributions tends towards 0 %, the greater the associated overestimation (i.e.

423 maximum 15.5 %) (Figure 5-a). The 'colour + geochemistry' model also provided a slight overestimation

424   of the contribution of mining tributaries (i.e. 7 % intercept of the regression line, Figure 5-b). Given the

425   slope of the regression line calculated is close to 1 (i.e. 0.98), this 7% overestimation remains constant

426   over the entire range of potential contributions.
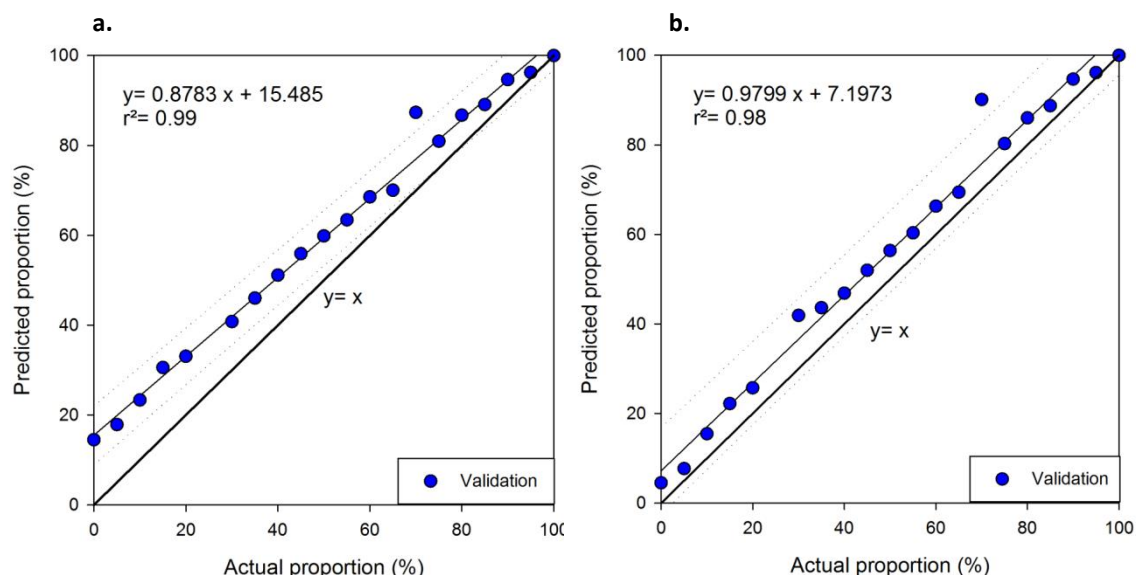
427   **Figure 5** Comparison between actual mining source proportions prepared in artificial mixtures and the mining
428   source proportions predicted by the 'geochemistry' (a) and 'colour + geochemistry' (b) models

429   **3.4 Building partial least-squares models based on FDVS**

430   Mining sources are characterized by a red-orange color while sediments originating from non-

431   mining sources are yellow-grey colour (Figure 1). The colour contrasts may be explained by the distinct

432   geochemical composition of these sources. Mean FDVS indicated the presence of goethite (i.e. at 445

433   and 525 nm), hematite (i.e. at 555, 565 and 575 nm), and organic matter (i.e. between 600-700 nm)

434   (Debret et al., 2011) in both mining and non-mining sources (Figure 6). In similar way, the Thio River

435   sediment samples (2015, 2017) showed similar characteristics since the variations of the mean FDVS

436   remained between those found in the sources (Figure 6). Nevertheless, some differences can be

437   observed between the sources. The spectral signature of goethite is slightly stronger at 445 nm in non-

438   mining tributaries compared to mining tributaries. No difference between sources was observed at

439   525 nm, the second wavelengths characterizing the presence of goethite. In contrast, the spectral

440 signature of hematite (*i.e.* at 555, 565 and 575 nm) was stronger in mining tributaries than in non-

441 mining tributaries.
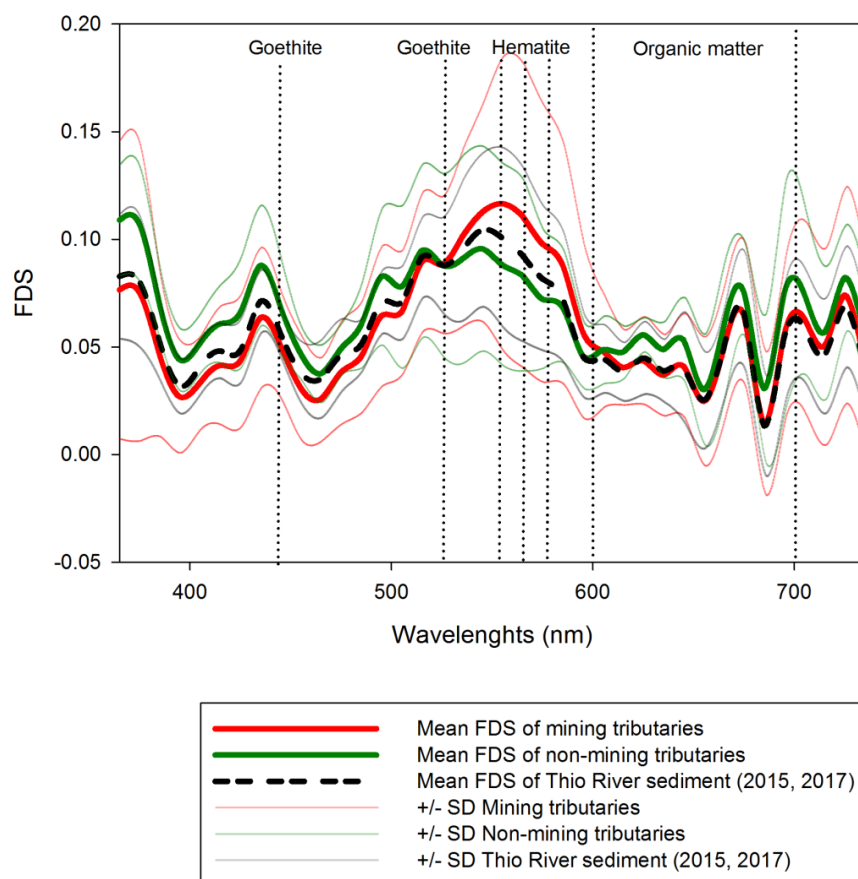
442 **Figure 6** FDVS measured in the <63 μm fraction of sources and Thio River sediment samples

443   To test the potential discrimination offered by FDVS, a PCA was applied on the source data set.

444 The first ten principal components from PCA explained 99 % of the total variation in the spectra. The

445 DFA performed on these components resulted in a final Wilks' lambda value of 0.1585. It means that

446 84.1 % of variance is explained by these ten components. Moreover, 100 % of the source samples were

447 correctly classified. The performances of FDVS-PLSR models are presented in Figure 7. The mining and

448 non-mining tributary FDVS-PLSR models provided an excellent correlation between actual and

449 predicted proportions with r² and slopes close to 1 and intercepts of linear regression close to 0. The

450 root mean square error of calibration (RMSEC) values estimated for both models were low, i.e. 3.4 %

451 and 3.1 % respectively for mining (Figure 7-a) and non-mining tributary models (Figure 7-b). These

452 models also provided a good predictability of source contributions with low root mean square error of

453 prediction (RMSEP) values (i.e. 8.0 % and 4.7 % respectively for mining and non-mining tributary

454 models). Another way to control the reliability of predictions was to sum the predicted proportions of

455 both models (Legout et al., 2013). Considering the whole data set used in the construction of the partial

456 least-squares regression models (i.e. calibration and validation) led to a mean sum of the predicted

457 source proportions of 102 % (SD 3 %, range: 98-114 %), thus highlighting the effective prediction

458 performance of FDVS-PLSR models.
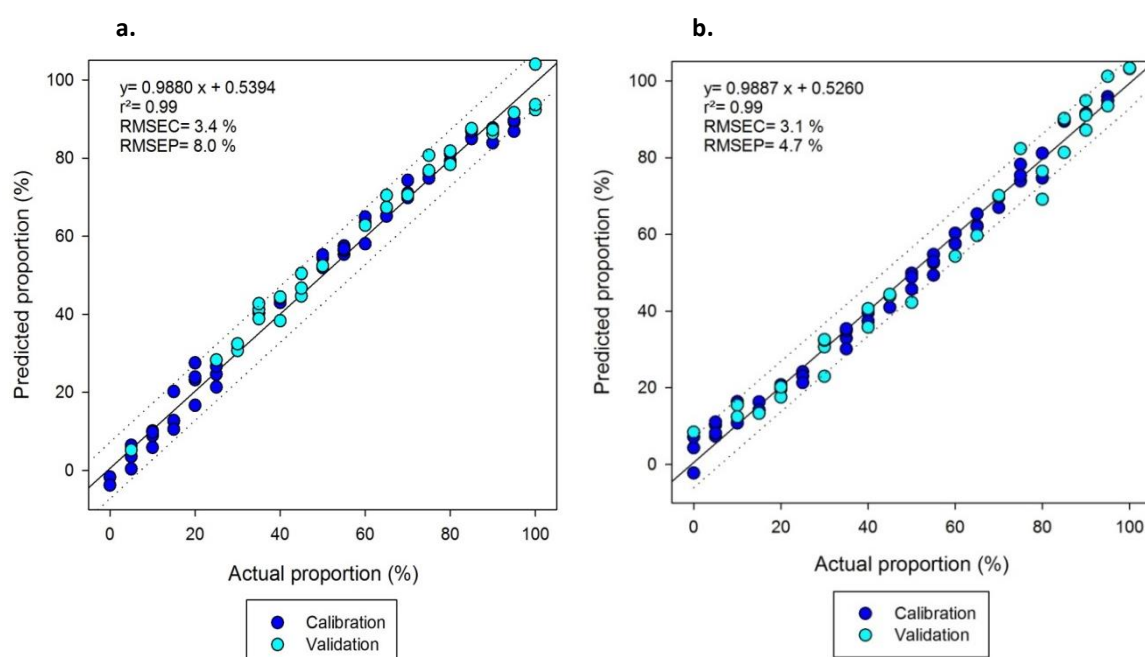
459 **Figure 7** Building of FDSV-PLSR models for mining sources (a) and non-mining sources (b)

460 **3.5 Source apportionment modelling**

461 3.5.1. 'Geochemistry' model

462 The 'geochemistry' model estimated that the mining tributaries contributed an average of 65

463 ± 27 % of the Thio River sediment during the 2015 flood event; they therefore dominated sediment

464 inputs overall during this event. Nevertheless, non-mining tributaries mainly contributed to the

465 sediment inputs at three sampling points along the Thio River (Figure 8-a, Table 4, sampling points [3,

466 5, 7]). These contributions did not, however, compensate for those provided by mining tributaries in

467   the estuary (63-89 %). Indeed, the dominant mining contributions found in upstream river reaches (96

468   %, Figure 8-a, Table 4, sampling point [1]) gradually decreased along the Thio River, fluctuating

469   between 17-77 % before increasing again at the confluence between the Thio River and the mining

470   tributaries draining the Thio Plateau mining area (i.e. 85 %, Figure 8-a, Table 4, sampling point [8]) and
       a.
471   reaching 60-64 %.

472

473   The 'geochemistry' model also demonstrated that mining tributaries dominated sediment inputs with

474   a mean contribution of 83 ± 8% during the 2017 flood event (Table 5). The lowest mining tributary

475   contributions estimated (i.e. 69 %) was found after the confluence with the Kouaré non-mining

476   tributary (Figure 8-b, Table 5, sampling point [4]). Nevertheless, further downstream, the proportions

477   of the mining sources increased again to reach 77-83 % in the estuary (Figure 6-b, Table 5, sampling

478   points [7, 8]).

479

480

481

482
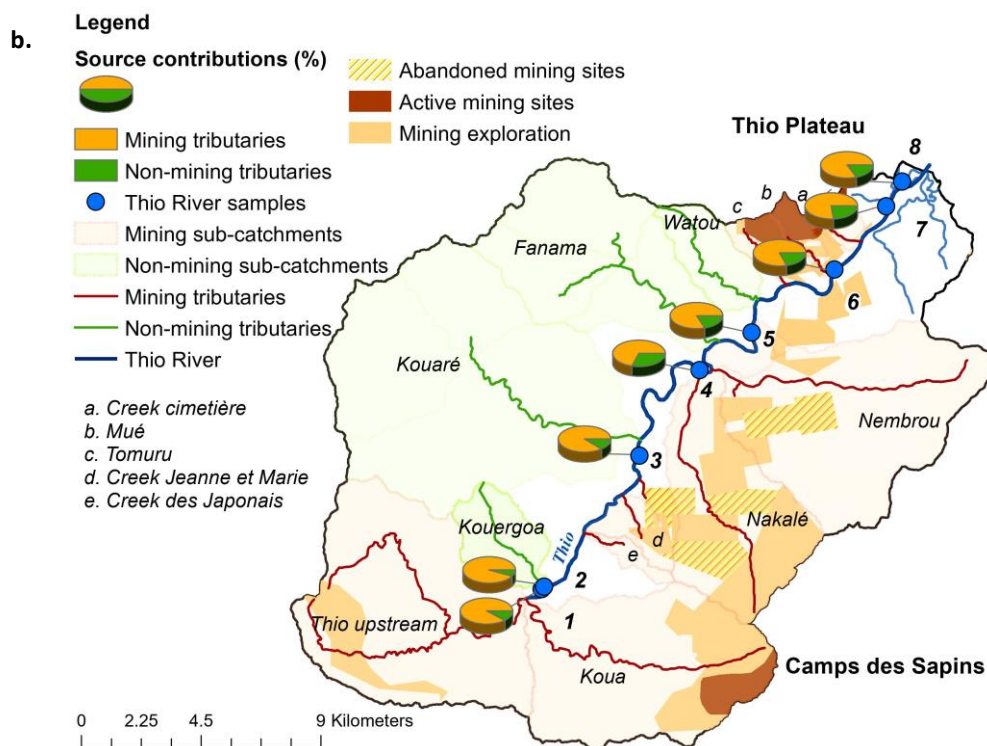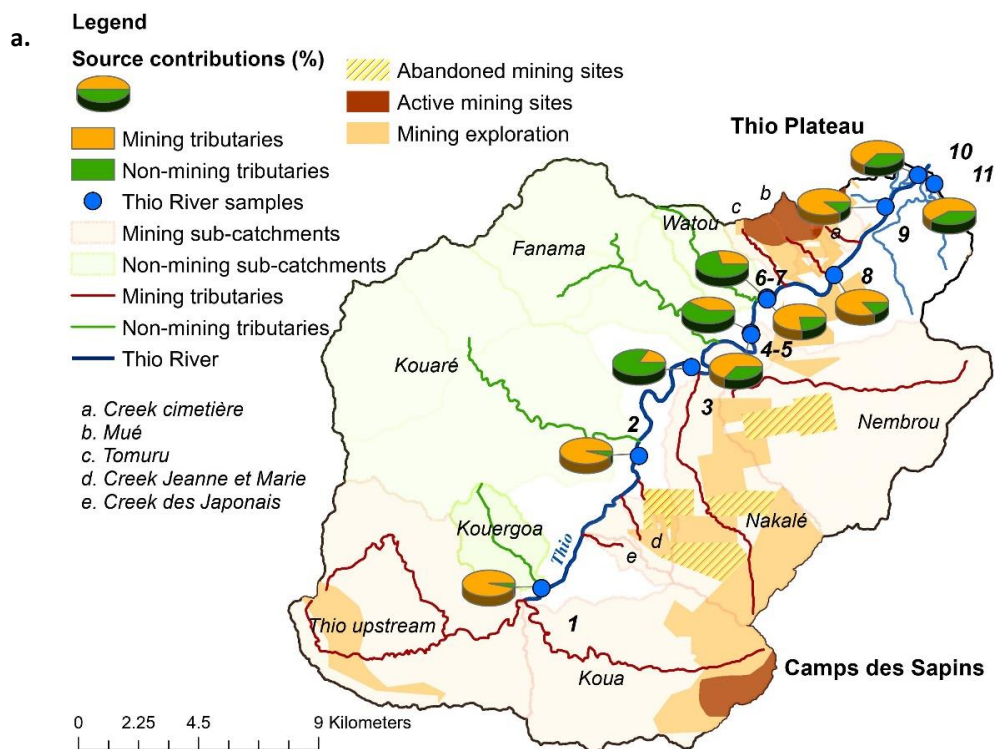
Figure 8 Relative contributions of mining and non-mining tributaries to the sediment collected in the Thio River during the 2015 (a) and 2017 (b) flood events using the 'geochemistry' model

485

486   3.5.2.   'Colour + geochemistry' model

487   Similar results were obtained with the 'colour + geochemisty' model. The contributions of

488   mining tributaries were estimated to an average of 68 ± 25 % for the 2015 flood event. Mining tributary

489   contributions provided almost all the sediment transiting the uppermost reach of the Thio River (i.e.

490   99 %, Figure 9-a, Table 4, sampling point [1]). However, after the confluence with the Kouaré tributary,

491   non-mining tributaries dominated with a contribution of 83 % (Figure 9-a, Table 4, sampling point [3]).

492   Further downstream, the contribution of mining tributaries increased again with supplies varying

493   between 34- 89 % to reach 58- 70 % in the estuary (Figure 9-a, Table 4). The largest difference between

494   'geochemistry' and 'colour + geochemistry' model outputs was 18 % for the 2015 flood event.

495   The 'colour + geochemistry' model also demonstrated that 88 ± 8 % of the sediment supply

496   originated from mining tributaries during the 2017 flood event. Along the Thio River, mining tributary

497   contributions varied between 100 % in the uppermost reach, 74% after the Kouaré river confluence

498   and 83-85% in the estuary (Figure 9-b, Table 5). The largest difference between 'geochemistry' and

499   'colour + geochemistry' model outputs was 10 % for the 2017 flood event (Table 5).

500

501

502

503
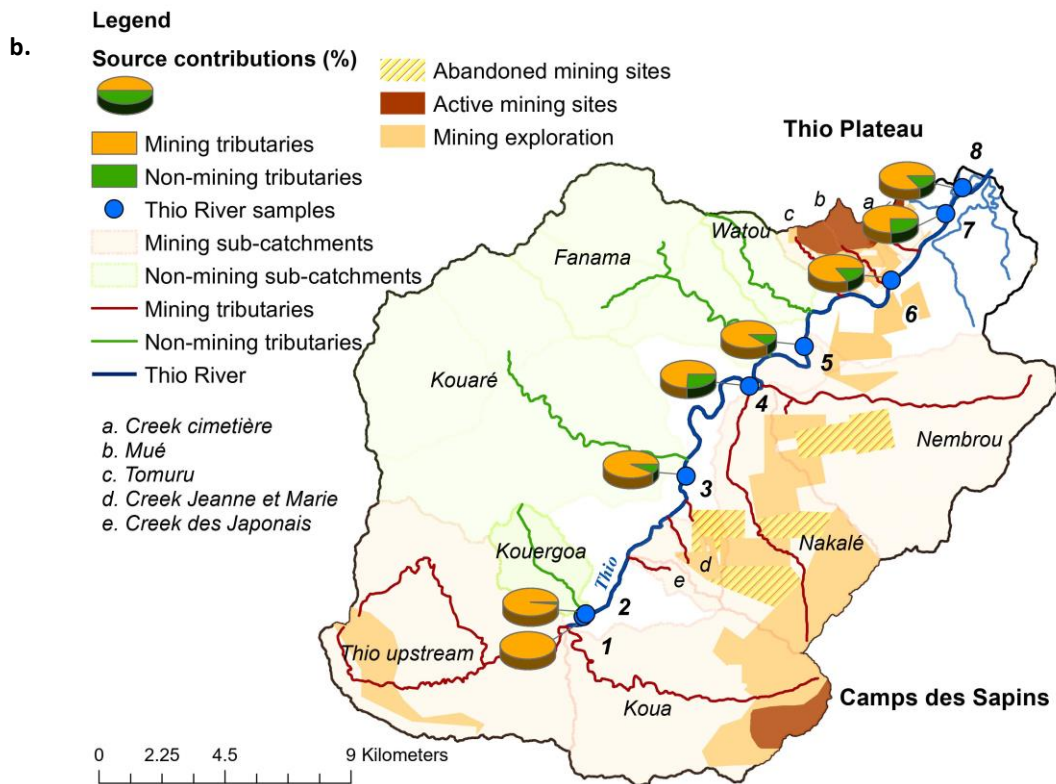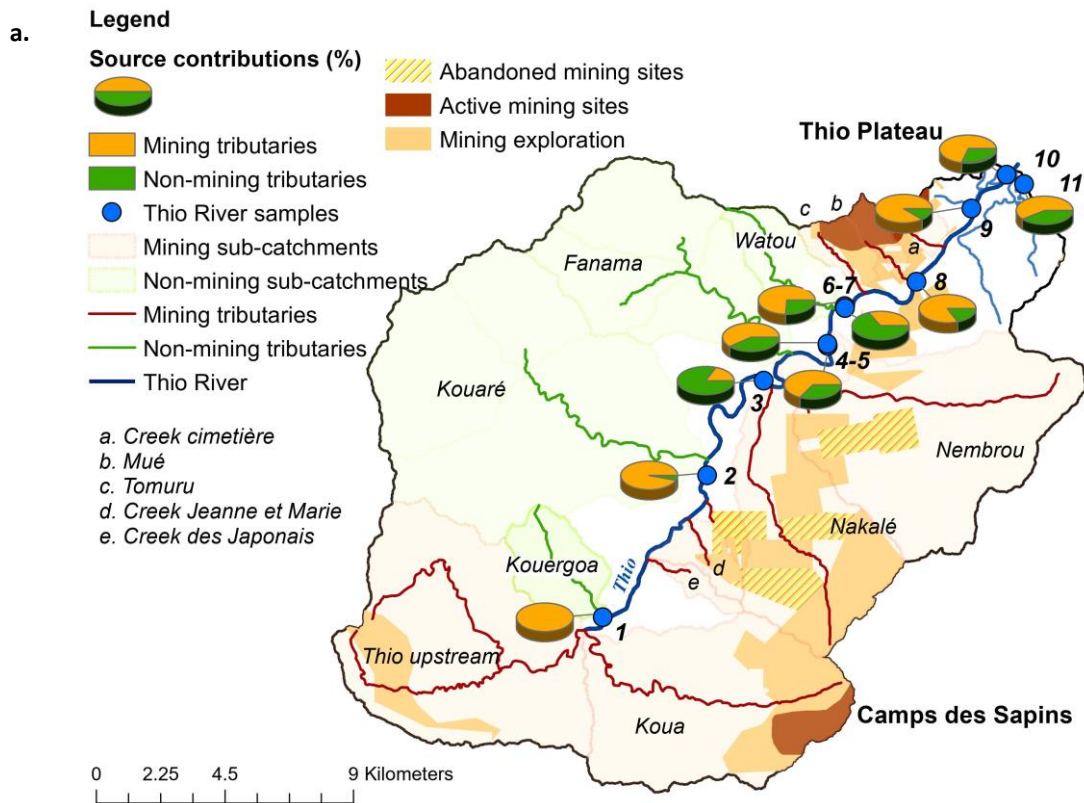
Figure 9 Relative contributions of mining and non-mining tributaries to the sediment collected in the Thio River
during the 2015 (a) and 2017 (b) flood events using the 'colour + geochemistry' model

506   3.5.3.   FDVS-PLSR model

507   Unlike the conventional fingerprinting approach, the estimated contributions of sources were

508 not limited to vary in the range between 0 % and 100 %. In a similar way, the sum of source

509 contributions was not constrained to be equal to 100 %. As a result, another way to control the

510 reliability of predictions was to sum the prediction proportions of both models. For example, if the

511 sum of the source contributions is close to 100 ± 20 % then it likely indicates that no source is lacking.

512 On the contrary, it is likely that a source has not been sampled and included in the study or that the

513 behaviour of the fingerprinting properties is not conservative (Legout et al., 2013). When applying the

514 FDVS-PLSR models (i.e. mining and non-mining tributary contributions) to the river sediment samples

515 (2015, 2017), the mean sums of the source contributions were 92 ± 8 % and 80 ± 13 %, respectively,

516 for the 2015 and 2017 flood events (Tables 4 and 5) which are satisfactory results. However, for the

517 2017 flood events, three river sediment samples collected on sampling points n°1, 2 and 3 showed

518 sums of source contributions below 70 %, indicating a lack of reliability of the model. The results

519 obtained on these three points must therefore be interpreted with great caution. Moreover, and owing

520 that predicted sums were slightly different from the expected 100 %, a bar plot display of the source

521 contributions has been chosen to facilitate the interpretation of the results (Figure 10).

522   According to the FDVS-PLSR model results, 34 ± 22 % of sediment supply originated from mining

523 tributaries while non-mining tributary contribution provided 58 ± 18 % of the sediment input for the

524 2015 flood event (Figure 10-a, Table 4). In the upper part of the Thio River catchment, non-mining

525 tributaries largely dominated with a contribution of 80 % versus 6 % for mining tributaries. Along the

526 Thio River, mining tributary contributions gradually increased to reach 70 % after the Mué tributary

527 confluence (i.e. one of tributaries draining the Thio Plateau Mine, Figure 8-a, Table 4, sampling point

528 [9]). The non-mining tributary contributions fluctuated along the Thio River between 41-85 % (Figure

529 8-a, Table 4, sampling points [2-8]) and reached a minimum to 28 % (Figure 10-a, Table 4, sampling

530 point [9]) after the Mué tributary confluence. In the estuary, sediment supply was originated from 51-

531   70 % of mining tributaries and 28-52 % of non-mining tributaries (Figure 10-a, Table 4, sampling points

532   [9, 10, 11]).

533   The FDVS-PLSR models also indicated that mining and non-mining tributaries respectively

534   contributed a mean of 29 ± 20 % and 51 ± 11 % of sediment (Figure 10-b, Table 5) during the 2017

535   flood event. In a similar way, mining contributions gradually increased along the Thio River from 11 %

536   in upper parts to reach 52-58 % in the estuary. On the contrary, non-mining contributions gradually

537   decreased from 56 % in uppermost parts to reach 35-36 % in the estuary (Figure 10-b, Table 5).

538   In summary, the FDVS-PLSR models provided opposite results to those of the conventional

539   sediment fingerprinting approach (i.e. 'geochemistry' and 'colour + geochemistry' models). According

540   to the FDVS-PLSR models, non-mining tributaries contributed the majority of the sediment supply for

541   the 2015 (58 ± 18 %) and 2017 (51 ± 11 %) flood events. On the contrary, the 'geochemistry' and 'colour

542   + geochemistry' models demonstrated that mining tributary contributions dominated sediment supply

543   for the 2015 (i.e. respectively 65 ± 27 % and 68 ± 28 %) and 2017 flood events (i.e. respectively 83 ± 8

544   % and 88 ± 8 %).

545

546

547

548
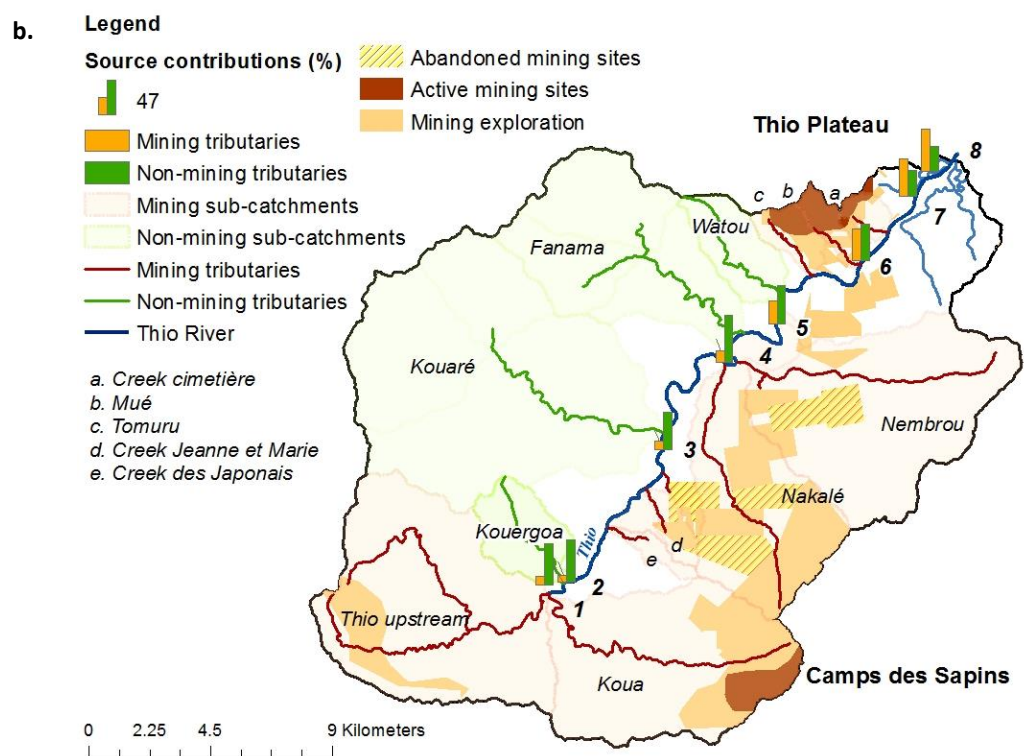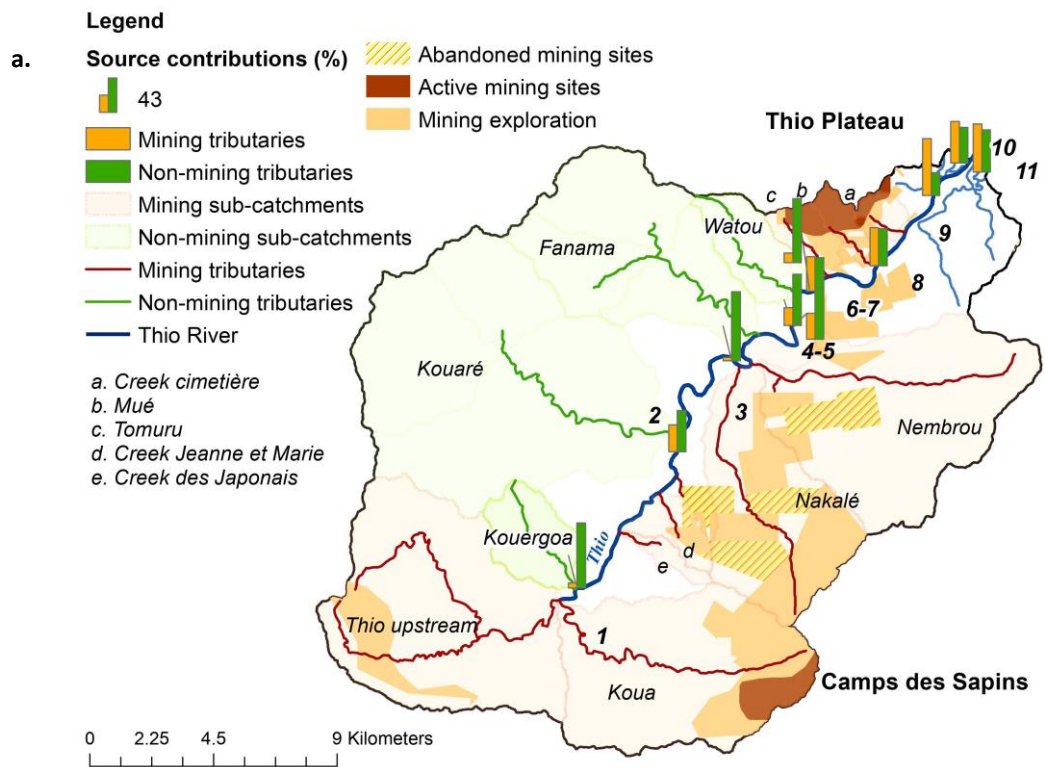
Figure 10 Relative contributions of mining and non-mining tributaries to the sediment collected in the Thio River during the 2015 (a) and 2017 (b) flood events using the FDVS-PLSR models

551   **Table 4** Source contributions calculated by FDVS-PLSR, 'geochemistry', 'colour + geochemistry' approaches for sediment deposited during the flood of February 25,2015

552   (Mean, SD: standard deviation, minimum, maximum)

Sampling point	Mining tributary contributions (%)			Non-mining tributary contributions (%)			Sum of source contributions (%) 553		
	FDS- PLSR	Geochemistry	Colour + Geochemistry	FDS- PLSR	Geochemistry	Colour + geochemistry	FDS- PLSR	Geochemistry	Colour 554 geochemistry
1	6	96	99	80	4	1	86	100	100 555
2	33	95	96	51	5	4	84	100	100
3	4	17	17	85	83	83	90	100	100
4	32	65	65	64	35	35	96	100	100
5	22	41	59	63	59	41	85	100	100
6	42	77	74	41	23	26	83	100	100
7	12	29	34	79	71	66	91	100	100
8	47	85	83	46	15	17	93	100	100
9	70	88	89	28	12	11	98	100	100
10	51	64	70	44	36	30	94	100	100
11	59	60	58	52	40	42	111	100	100
Mean (%)	34	65	68	58	35	32	92	100	100
SD (%)	22	27	25	18	27	25	8	-	-
Minimum (%)	4	17	17	28	4	1	84	-	-
Maximum (%)	70	96	99	85	83	83	111	-	-

556 **Table 5** Source contributions calculated by FDVS-PLSR, 'geochemistry', 'colour + geochemistry' approaches for sediment deposited during the flood of April 10,2017 (Mean,
557 SD: standard deviation, minimum, maximum)

Sampling point	Mining tributary contributions (%)			Non-mining tributary contributions (%)			Sum of source contributions (%)		
	FDS- PLSR	Geochemistry	Colour + Geochemistry	FDS- PLSR	Geochemistry	Colour + geochemistry	FDS- PLSR	Geochemistry	Colour + geochemistry
1	11	90	100	56	10	0	66	100	100
2	9	94	98	58	6	2	68	100	100
3	11	89	92	52	11	8	63	100	100
4	16	69	74	66	31	26	82	100	100
5	32	82	89	54	18	11	86	100	100
6	44	81	84	51	19	16	95	100	100
7	52	77	83	36	23	17	88	100	100
8	58	83	85	35	17	15	92	100	100
Mean (%)	29	83	88	51	17	12	80	100	100
SD (%)	20	8	8	11	8	8	13	-	-
Minimum (%)	9	69	74	35	6	0	63	-	-
Maximum (%)	58	94	100	66	31	26	95	-	-

558

3.6 Complementary tests: representativeness of artificial mixture samples used for the FDVS-PLSR models compared to source samples

The FDVS-PLSR models provided contradictory results compared to those obtained with the 'geochemistry' and 'colour + geochemistry' models. In order to explain these results, complementary analyses were carried out with this model. This model was built from the mining and non-mining tributary samples (i.e. mixture of source samples > source poles > artificial mixture samples > FDVS-PLSR models). The objective of these analyses was to check whether the model is 'well built', in other words whether it is representative of the sources identified and whether it is capable of correctly 'classifying' the sources. To this end, we applied the FDVS-PLSR models on source samples to estimate their composition in terms of source contributions with FDVS-PLSR models. In the same way as we did above for the river sediment samples, we assessed the reliability of predictions by summing the source contributions predicted by both models (Legout et al., 2013). A mean sum of the predicted source proportions of 94 ± 17 % was calculated from the source sample data set which again is an excellent result. However, for the three mining tributary samples collected on the Koua tributary, the corresponding sums remained below 65 % with a minimum of 49% whereas for one of the non-mining tributary sample collected on the Kouaré tributary, the sum reached 131% (Figure 11). These results indicate that the FDVS-PLSR models provide unreliable predictions when dealing with river sediment samples with a colour signature partly due to these four samples. The colorimetric signature of the mining tributary samples collected on the Koua tributary in particular is not fully recognized by the models. The compositions of mining and non-mining tributary samples in Figures 11 and 12 also show that artificial mixture samples built from a mix between the composite mining source sample and the composite non-mining source sample did not cover entirely the range of values found in all the sources samples which may explain why some source samples showed mining and non-mining tributary composition lower than 0 and/or higher than 100 %.

583
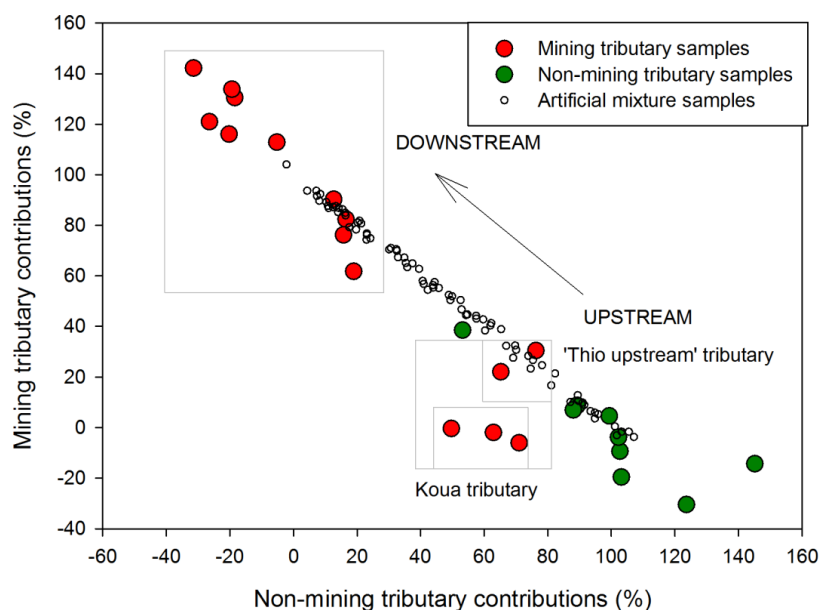
Figure 11 Relative compositions of mining and non-mining sources estimated by the FDVS-PLSR models applied to the individual source sediment samples

584

585

586   Moreover, we observed that two sub-groups of mining tributary samples can be distinguished,

587   the first one corresponding to samples collected on the mining tributaries located in the uppermost

588   part of the catchment and the second to samples collected on the mining tributaries located further

589   downstream. The FDVS-PLSR differentiated rather well the second group since the mining tributary

590   composition is dominant in these samples. On the contrary, the first group referred to as 'Upstream'

591   merged with the non-mining tributary samples (Figure 11). Indeed, Figure 12 shows the mining

592   tributaries located in the upper part of the catchment were defined as 'non-mining tributaries' by the

593   FDVS-PLSR models.

594
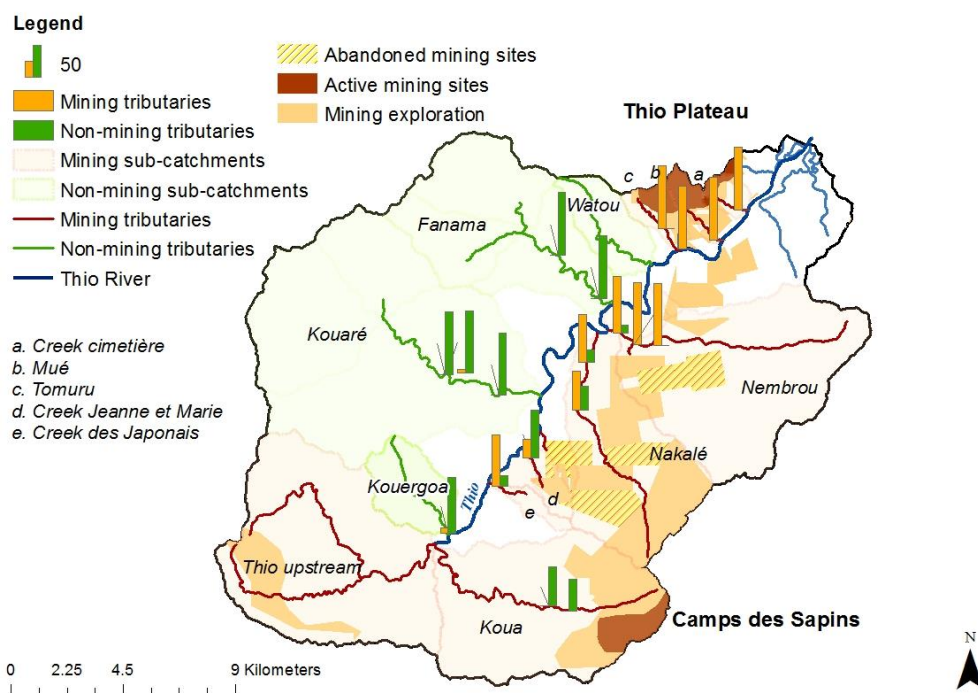
Figure 12 Relative compositions of mining and non-mining sources estimated by the FDVS-PLSR models applied to the individual sediment sources in the Thio River catchment

The low K contents found in these samples confirmed, however, that they were mainly supplied by mining sources (Figure 13). Indeed, only tributaries draining peridotite massifs (i.e. mining areas) can show such low K contents in source samples (Sellier et al., 2019). Nevertheless, a colour difference could be observed visually and through variations of the a* parameter: the a* values increased from upper parts to lower, which results in an increasingly red coloration of mining tributary samples in downstream direction. Figure 13 shows also that the a* values found in samples collected in the upper catchment part overlapped with those of non-mining tributary samples.
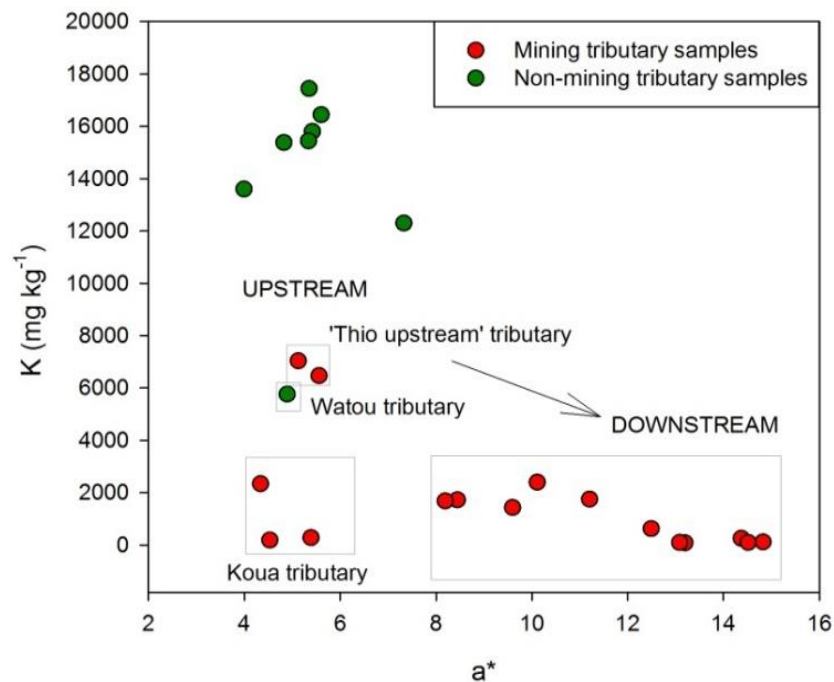
604   **Figure 13** Diagram of K contents as a function of a* parameter values within sediment sources and artificial

605   mixture samples

606   **4.Discussion**

607   **4.1.Advantages and limits of models**

608   4.1.1.   'Colour' model

609   One of the objectives of this study was to test the contribution of spectrocolorimetry for

610   improving the source discrimination. Indeed, visual observations indicated that mining tributary

611   samples were red-orange whereas non-mining tributary samples were rather yellow-grey (Figure 1).

612   However, the results showed that the colour parameters, when used individually, did not provide

613   sufficient discrimination between sources (Table 2) to meet this objective. Indeed, some mining

614   tributary samples showed colour parameter values similar to those found in non-mining tributary

615   samples (e.g. v' at Table 3, or a* shown at Figure 13). This overlap of value ranges could explain in

616   particular the inability of the 'colour' model to provide satisfactory source discrimination. In the case

617   of mining sources, minerals such as hematite or goethite provide them their reddish-orange colour

618   (Quantin et al., 1997). Indeed, hematite is a red coloured oxidized mineral while goethite is a yellow

619   coloured oxidized mineral (Trescases, 1973). According to Figure 6, non-mining tributary samples also

620   have high contents of goethite which could interfere with the discrimination of the colour signatures

621   of the two sources. The non-mining tributaries drain areas devoid of mining activities mainly located

622   on the volcano-sedimentary formation rocks. The soil-geological profiles within the volcano-

623   sedimentary formation rocks are characterized at the surface by clay horizons and at depth by oxidized

624   horizons enriched in goethite in particular (Denis, 1988). According to Sellier et al. (2019), subsurface

625   erosion processes dominate in the Thio River catchment. In other words, landslides mainly contribute

626   to non-mining sediment inputs. As a result, the oxidized horizons of these rock formations are also

627   likely subject to erosion processes which could explain the occurrence of goethite and material with a

628   yellow-grey color in non-mining tributary samples.

629

630   Moreover, results obtained with colour parameter analyses coupled to visual observations

631   highlighted the occurrence of two groups of mining tributary samples (i.e. 'Upstream' and

632   'Downstream'). The coloration differences (i.e. orange/ 'Upstream' and 'red/Downstream') observed

633   between these two groups could be due to the the fact that on the one hand, the reddish colour does

634   not provide a highly conservative signature as it may be altered by the oxydo-reduction of iron minerals

635   during the periods of submersion of sediments under water. On the other hand, the presence of

636   different types of nickel ores could explain these coloration differences. Indeed, the laterite profile is

637   classically described in the literature as composed of peridotites at the bottom > saprolites > yellow

638   laterites rich in goethite > red laterites rich in hematite at the top (Trescases, 1973). However, certain

639   minor features may be found in the laterite profile depending on the type of parent rock found at the

640   base of the peridotite massifs (Sevin, 2014). The mineral composition found in the different layers of

641   the laterite profile may vary depending on whether serpentines or peridotites are the source rocks.

642   Moreover, nickel ore formation depends partly on the morphological context, for instance on whether

643   nickel ores are located in a basin, on a plateau or a slope. This morphological context influences the

644   weathering level of peridotites and the formation of laterite profile: the more the laterite profile is

645   altered, the higher the thickness of red laterites. In the Thio River catchment, nickel ores from the Thio

646   Plateau mine located in the downstream part of the catchment are 'plateau nickel ores' whereas those

647   from the Camps des Sapins mine located in the upstream part of the catchment are 'slope nickel ores'

648   (Mardhel et al., 2018). No information is provided in the literature on the types of nickel ores that were

649   mined in abandoned mining sites. The red coloration of the 'Downstream' mining tributary samples

650   could then be associated with more altered laterite profiles with a thicker layer of red laterites

651   characteristic of 'plateau nickel ores' compared to the 'Upstream' mining tributary samples, which

652   could be associated with a laterite profile with a thinner layer of red laterites characteristic of 'slope

653   nickel ores'. The red laterites are the final stage of alteration of the peridotite massifs. It therefore

654   appears likely that the less altered 'slope nickel ore' probably contains more yellow laterites enriched

655   in goethite compared to the 'plateau nickel ore'. This hypothesis could explain the similar colour

656   signature of the mining tributary samples collected on the Koua tributary draining the Camps des

657   Sapins mine and the non-mining samples.

658   4.1.2. 'Geochemistry' model

659   The 'geochemistry' model based on K provided significant discrimination between sources

660   (Table 2), regardless of the types of nickel ores that may be found in the Thio River catchment. K is a

661   lithological tracer discriminating sediments originating from the erosion of the two dominant

662   lithologies (i.e. peridotite massifs vs. volcano-sedimentary formations) in the Thio River catchment. As

663   anthropogenic erosion (i.e. due to mining activities) dominates on the peridotite massifs (Garcin et al.,

664   2017), K therefore provides an optimal discrimination between mining and non-mining tributary

665   contributions.

666   This parameter classified the source samples rather well (i.e. 95.3 % of correct classification,

667   Table 3). Indeed, the 16 mining source samples were all correctly classified (100%) and only one non-

668   mining source sample was not correctly classified (87.5 %); it corresponds to the Watou tributary

669   sample (Figure 13). This sample showed a K content similar to that found in mining tributary samples.

670   The Watou tributary is particular because it drains both volcano-sedimentary formations and

671   peridotite massifs that were not exploited for mining, which justifies that it was considered as a non-

672   mining tributary. The K content measured in this sample could be representative of that found in

673   sediment sources characterized by a mix between the two dominant lithologies. Again, when observing

674   Figure 13, two mining tributary samples (i.e. 'Thio upstream') showed similar K contents to that found

675   in the Watou tributary sample. The 'Thio upstream' tributary also drains both areas associated with

676   volcano-sedimentary formations and exploited peridotite massifs (i.e. mining prospection), which

677   justifies that it was considered as a mining tributary.

678   The analysis of colour parameters coupled with that of geochemical elements indicated that

679   these samples collected on the 'Thio upstream' tributary showed a less red coloration not because

680   they are associated with a different type of ore, as could be the case for the samples collected on Koua

681   tributary draining Camps des Sapins mine (Figure 13), but because they are characterized by a mix of

682   both lithologies. As a result, the 'geochemistry' model showed a certain limitation to classify source

683   samples characterized by a mix of both lithologies. The performance of the 'geochemistry' model

684   described in Table 2 remains, however, excellent. The application of this model on artificial mixture

685   samples provided very satisfactory results (Figure 5-a) with a good correlation between the predicted

686   and the actual source proportions (r^2= 0.99). Estimations of mining tributary contributions may,

687   however, be overestimated. This overestimation evaluated to a maximum at 15.5 % is greater when

688   the mining contributions estimated by the model tend towards 0 % (maximum: 15.5 %, Figure 3-a).

689   The 'geochemistry' model has difficulties to discriminate sediment contributions from sub-catchments

690   with mixed lithologies. It classifies these types of samples as originating from mining tributaries, such

691   as the Watou River sample. As a result, as the K concentrations decrease in the samples analyzed, the

692   model will tend to overestimate the contributions of mining sources by default compared to their

693   actual contributions.

694

### 4.1.3.	'Colour + geochemistry' model

The 'colour + geochemistry' (i.e. K, Ca, Ti, b*, C*) model provided the best discrimination between sources (Table 3). The inclusion of colour parameters in the 'colour + geochemistry' approach allowed for the discrimination of source samples (i.e. 100 % of correctly classified source samples) that a 'geochemistry' approach alone could not achieve. Results of the tests carried out on the artificial mixture samples also showed an excellent correlation between the predicted and the actual source proportions (i.e. r^2= 0.98). A slight overestimation of the mining tributary contributions (7 %) was observed with this approach, which remains rather reasonable (Figure 3-b). In this model, K is the lithological tracer which has the higher discriminant powerful (Table 2), which may explain the similarity of results obtained with the 'colour + geochemistry' and the 'geochemistry' models. Indeed, mining tributaries contributed an average of 65 ± 27 % for 'colour + geochemistry' model and 68 ± 25 % for 'geochemistry' model (Table 4). For the 2017 flood event, mining source contributions largely dominated the sediment production with a mean contribution of 83 ± 8 % for the 'geochemistry' model and 88 ± 8 % for the 'colour + geochemistry' model.

### 4.1.4.	FDVS-PLSR models

The FDVS-PLSR models built from artificial mixture samples showed excellent theoretical predictive performances (e.g. r^2, RMSEC, RMSEC, Figure 7). However, the application of these models on river sediment samples provided questionable results. Indeed, the artificial mixture samples did not cover entirely the ranges of values found in all sources samples, thus resulting in an overestimation (i.e. superior to 100 %) and an underestimation (i.e. inferior to 0 %) of source composition (Figure 11) in several source samples. Similarly to what was previously observed, three sub-groups of mining tributary samples can be distinguished, one of which (i.e. 'Thio Upstream') is partially merged with the non-mining tributary samples (Figure 11). When modelling the source contributions with the FDVS-PLSR models, a bias was created because the contributions of the 'Thio upstream' tributary may be mainly considered as the contributions of non-mining tributaries. As a result, an overestimation of non-

720   mining tributary contributions may be found in the entire Thio River catchment and particularly in the

721   upper part of the study area. Third, the properties measured in the Koua tributary (i.e. draining Camps

722   des Sapins Mine) samples were not comprised in the ranges of values covered by the artificial mixture

723   samples (Figure 11).

724   Given the particular colour signature of this tributary (Figure 13), its contributions are therefore

725   not taken into account at all by the FDVS-PLSR models. Indeed, the sums of the source contributions

726   by FDVS-PLSR models are lower than the expected 100% particularly in the uppermost part of the

727   catchment (Tables 4 and 5), which may indicate that a source is not accounted for. Artificial mixtures

728   were constructed from a homogenized spectral signature of all mining source samples. However, two

729   distinct spectral signatures were observed between the upstream and downstream mining source

730   samples. Homogenizing the spectral signature of the mining samples led to a loss of information in

731   terms of spectral signature, in particular that of the mining samples located upstream. As a result, a 3-

732   source FDVS-PLSR models (i.e. non-mining, upstream and downstream mining sources) would have

733   been more appropriate than 2-source FDVS-PLSR models in this context.

4.2. Spatial and temporal variations of sediment source contributions

735   Among the four models tested in this study, the 'colour + geochemistry' model is the most

736   appropriate to estimate mining and non-mining tributary contributions in the Thio River catchment.

737   According to the results of this model, mining tributaries provided the main sediment supply to the

738   river system with a mean contribution of 68 ± 25 % for the 2015 flood event and 88 ± 8 % for the 2017

739   flood event (Tables 4 and 5). The variability of mining tributary contributions between these two flood

740   events with a return period of 10 years (3500 $m^3 s^{-1}$) could be explained in particular by the variability

741   of rainfall distribution (Sellier et al., 2019). Indeed, during the 2015 flood event, the Kouaré River sub-

742   catchment received twice the rainfall than observed in the rest of the Thio River catchment, which may

743   explain a higher contribution of non-mining tributaries for this event than for the 2017 flood event

744   where rainfall was more intense on the eastern part of the catchment in the vicinity of the mines

745 currently in operation (Thio Plateau, Camps des Sapins). In addition, the inhabitants of Thio reported

746 that bushfires had occurred in the Kouaré and Fanama sub-catchments in 2015, which could have led

747 to an increase in soil erosion processes, particularly landslides, in these sub-catchments. This could

748 also explain why the sediment contributions of the Kouaré tributary are higher in 2015 compared to

749 2017. However, it is likely that, as for low intensity floods (i.e. <200 $m^3.s^{-1}$), sediment generated during

750 previous floods has been remobilized (Allenbach et al., 2020). The current research does not allow to

751 quantify this proportion of remobilized sediments. Future studies based on the measurement of the

752 $^7Be/^{210}Pb_{xs}$ ratio could provide information on this question as both isotopes are supplied by rainfall

753 and ^7Be is short-lived while $^{210}Pb_{xs}$ is much longer-lived. Indeed, this ratio has been used in previous

754 research to determine whether sediment has been eroded recently (i.e. with a high ratio of $^7Be/^{210}Pb_{xs}$)

755 or whether they have been remobilized from the channel (i.e.with a low ratio of $^7Be/^{210}Pb_{xs}$) (Le Gall et

756 al., 2017;Evrard et al., 2015).

757 Although the FDVS-PLSR models were unable to properly estimate the source contributions,

758 they provided qualitative indications about the proportion of sediment contribution between

759 'Upstream' and 'Downstream' mining tributaries at the level of the estuary. Indeed, only 'downstream'

760 mining tributaries were finally identified by the FDVS-PLSR models as mining sources. Mining

761 contributions gradually increased in downstream direction. The predicted proportion sums of river

762 sediment samples also tend to reach the expected 100 %, which could result in a better predictability

763 of the models. As a result, these models indicated that sediment contribution from downstream

764 reaches dominated that of upstream reaches at the level of the estuary for both events.

765 Moreover, the analysis of colour parameters coupled to that of geochemical elements

766 highlighted the occurrence of three sub-groups of mining tributary samples, (1) 'Downstream' samples

767 characterized by high a* values and low K contents, (2) 'Koua tributary' samples located in the

768 upstream characterized by low a* values and low K contents and (3) 'Thio upstream' samples

769 corresponding to a mix of both dominant lithologies (i.e. peridotite massifs and volcano-sedimentary

770   formations) characterized by low a* values and higher K contents (i.e. 4 times higher than for the two

771   previous sub-groups) (Figure 13). Owing to the low K contents found in Thio River sediment samples

772   collected in the uppermost part (i.e. ~ 2200 mg kg^{-1} in 2015 and ~ 2600 mg kg^{-1} in 2017), which were

773   similar to those measured in samples of sub-group (2) (~2400 mg kg^{-1}), it would appear that the Koua

774   tributary draining Camps des Sapins mine dominated the sediment supply in the upstream for both

775   events.

Conclusions

777   The current study showed that the contributions of mining sources dominated the sediment

778   inputs with mean contributions of 68 ± 25 % for the 2015 flood event and 88 ± 8 % for the 2017 flood

779   event (results of 'colour + geochemistry' model). Although the spatial variability of rainfall may impact

780   local sediment source contributions, a trend in terms of sediment source contributions is observed

781   along the Thio River for both flood events. In the uppermost part of the catchment, mining source

782   contributions dominated (99% in 2015, 100% in 2017) with a dominant contribution from the Koua

783   tributary draining the Camps des Sapins mine. The first non-mining tributary encountered in

784   downstream direction (i.e. the Kouergoa tributary) contributed little to sediment supply; it is rather

785   the next non-mining tributaries (i.e. the Kouaré tributary) which provided most of the sediment inputs

786   (83 % in 2015, 26 % in 2017). Nevertheless, these contributions were compensated in downstream

787   direction by those from mining sources generated by tributaries draining Thio Plateau mine. Finally, at

788   the estuary, mining sources dominated (58-70 % in 2015, 83-85 % in 2017). These results therefore

789   suggest that catchment management should focus on mining tributaries draining active mining sites

790   (i.e. Camps des Sapins and the Thio Plateau) and the Kouaré tributary for the non-mining tributaries.

791   One of the objectives of this study was to evaluate the performance of sediment tracing

792   methods based on spectroscopy measurements (i.e. colour parameters and FDVS). The results showed

793   that these individual fingerprinting approaches did not provide sufficient discrimination between

794   sources to be used for the modelling of sediment source contributions. Nevertheless, the inclusion of

795 colour properties in addition to geochemical parameters turned out to be the optimal combination of

796 tracers providing the highest discrimination between sediment sources. This 'colour + geochemistry'

797 model is, however largely based on the discriminatory power provided by K, which means that the

798 'geochemistry' approach is also relevant to quantify sediment sources. Both approaches have,

799 moreover, been experimentally validated. As a result, the use of these approaches could be extended

800 to other mining catchments of New Caledonia but also possibly to other similar nickel mining

801 catchments (i.e. Ni oxidized ores based on peridotite massifs) around the world.

802 **Data availability**

803 The database has been registered on the PANGEAE website and is currently undergoing the

804 editorial process: https://issues.pangaea.de/browse/PDI-25229.

805 **Author contribution**

806 Oldrich Navratil, Michel Allenbach and Olivier Evrard designed research. Virginie Sellier, Oldrich

807 Navratil, Olivier Evrard and Irène Lefèvre carried out fieldwork sampling. Virginie Sellier conducted the

808 analyses. All co-authors contributed to data analysis and interpretation. John Patrick Laceby

809 contributed to modelling. All co-authors contributed to the writing and approved the final version of

810 the manuscript.

811 **Competing interests**

812 The authors declare that they have no conflict interest.

813 **Acknowledgements**

814 This work was funded by the National Technical Research Center (CNRT) "Nickel and Its Environment",

815 Noumea, New Caledonia » (n°10PS2013-CNRT.UNC/IMMILA). The PhD project of Virginie Sellier is also

816 financed by the French Atomic Energy Commission (CEA, Commissariat à l'Energie Atomique et aux

817   Energies Alternatives). The authors are grateful to Jean-Guy M'Boueri, Pierre Chanel, Jean-Jean,

818   Lorenza M'Boueri, Nicolle Mathys for their invaluable support to identify and have access to the field

819   sampling sites. The authors would also like to thank Magdalena Uber for her contribution to the

820   spectrocolorimetric analyses.

821

822 **References**

823 Abel, A., Michael, A., Zartl, A., and Werner, F.: Impact of erosion-transported overburden dump materials
824   on water quality in Lake Cospuden evolved from a former open cast lignite mine south of Leipzig,
825   Germany, Environmental Geology, 39, 683-688, 2000.

826 Allenbach, M., Bertrand, M., Despinoy, Y., Evrard, O., Garcin, M., Liébault, F., Navratil, O., Recking, A.,
827   Richard, D., Rouet, I., Sabinot, C., Sellier, V., Tessier, B., Thinon, I., Touraivane, and Worliczek, E.:
828   Rapport scientifique. Programme « IMMILA, Impact de la mine au lagon ». CNRT « Nickel & son
829   environnement. 250 pages. , 2020.

830 Batista, P. V. G., Laceby, J. P., Silva, M. L. N., Tassinari, D., Bispo, D. F. A., Curi, N., Davies, J., and Quinton,
831   J. N.: Using pedological knowledge to improve sediment source apportionment in tropical
832   environments, J Soils Sediments, 10.1007/s11368-018-2199-5, 2018.

833 Baudrimont, M., Dominique, Y., Feurtet-Mazel, A., Gonzalez, P., Gourvès, P.-Y., Gunkel-Grillon, P., Laporte-
834   Magoni, C., Lefrançois, E., Letourneur, Y., Marquié, J., Maury-Brachet, R., Monna, F., Pasquet, C.,
835   Rivière, E., and Roth, E.: - Rapport scientifique final. Programme « Dispersion des métaux de la mine
836   au lagon. ». CNRT « Nickel & son environnement ». 192 pages, 2019.

837 Bird, E. C. F., Dubois, J. P., and Iltis, J. A.: The impacts of opencast mining on the rivers and coasts of New
838   Caledonia. Tokyo, Japan, United Nations University, 1984.

839 Blake, W. H., Wallbrink, P. J., Wilkinson, S. N., Humphreys, G. S., Doerr, S. H., Shakesby, R. A., and Tomkins,
840   K. M.: Deriving hillslope sediment budgets in wildfire-affected forests using fallout radionuclide tracers,
841   Geomorphology, 104, 105-116, 10.1016/j.geomorph.2008.08.004, 2009.

842 Brosinsky, A., Foerster, S., Segl, K., and Kaufmann, H.: Spectral fingerprinting: sediment source
843   discrimination and contribution modelling of artificial mixtures based on VNIR-SWIR spectral
844   properties, Journal of soils and sediments, 14, 1949-1964, 2014.

845 Brown, A.: The potential use of pollen in the identification of suspended sediment sources, Earth Surface
846   Processes and Landforms, 10, 27-32, 1985.

847 Clarke, P., and David, C.: New Provincial Environmental Legislation in New Caledonia: Continuity and
848   Reform in Environmental Governance in a French Pacific Territory, Asia Pac. J. Envtl. L., 13, 135, 2010.

849 Collins, A., and Walling, D.: Selecting fingerprint properties for discriminating potential suspended
850   sediment sources in river basins, Journal of hydrology, 261, 218-244, 2002.

851 Collins, A. L., Walling, D. E., and Leeks, G. J. L.: Composite fingerprinting of the spatial source of fluvial
852   suspended sediment : a case study of the Exe and Severn river basins, United Kingdom,
853   Géomorphologie, 2, 41-53, 10.3406/morfo.1996.877, 1996.

854 Coulthard, T. J., and Macklin, M. G.: Modeling long-term contamination in river systems from historical
855   metal mining, Geology, 31, 451-454, 2003.

856 Danloux, J., and Laganier, R.: Classification et quantification des phénomènes d'érosion, de transport et
857   de sédimentation sur les bassins touchés par l'exploitation minière en Nouvelle Calédonie, 1991.

858 Daszykowski, M., Walczak, B., and Massart, D.: Representative subset selection, Analytica chimica acta,
859   468, 91-103, 2002.

860 Davis, C. M., and Fox, J. F.: Sediment fingerprinting: review of the method and future improvements for
861   allocating nonpoint source pollution, J Environ Eng, 135, 490-504, 2009.

862 Debret, M., Sebag, D., Desmet, M., Balsam, W., Copard, Y., Mourier, B., Susperrigui, A.-S., Arnaud, F.,
863   Bentaleb, I., and Chapron, E.: Spectrocolorimetric interpretation of sedimentary dynamics: the new
864   "Q7/4 diagram", Earth-Science Reviews, 109, 1-19, 2011.

865 Denis, B.: Etude de sols fersiallitiques désaturés du plateau de Tango (Nouvelle-Calédonie), Cahiers
866   ORSTOM. Série Pédologie, 24, 61-76, 1988.

867 Dumas, P.: Méthodologie de cartographie de la sensibilité des sols à l'érosion appliquée à la région de
868   Dumbéa à Païta-Bouloupari (Nouvelle-Calédonie), Les Cahiers d'Outre-Mer. Revue de géographie de
869   Bordeaux, 63, 567-584, 2010.

870 Dumas, P., Printemps, J., Mangeas, M., and Luneau, G.: Developing erosion models for integrated coastal
871   zone management: A case study of The New Caledonia west coast, Marine Pollution Bulletin, 61, 519-
872   529, 2010.

873 Evrard, O., Laceby, J. P., Huon, S., Lefèvre, I., Sengtaheuanghoung, O., and Ribolzi, O.: Combining multiple
874   fallout radionuclides (137Cs, 7Be, 210Pbxs) to investigate temporal sediment source dynamics in
875   tropical, ephemeral riverine systems, J Soils Sediments, 16, 1130-1144, 10.1007/s11368-015-1316-y,
876   2015.

877 Evrard, O., Durand, R., Foucher, A., Tiecher, T., Sellier, V., Onda, Y., Lefèvre, I., Cerdan, O., and Laceby, J.
878   P.: Using spectrocolourimetry to trace sediment source dynamics in coastal catchments draining the
879   main Fukushima radioactive pollution plume (2011–2017), Journal of Soils and Sediments, 1-12, 2019.

880 Evrard, O., Chaboche, P.-A., Ramon, R., Foucher, A., and Laceby, J. P.: A global review of sediment source
881   fingerprinting research incorporating fallout radiocesium (137Cs), Geomorphology, 107103, 2020.

882 Garcin, M.: Exploitation des granulats en lit vif des cours d'eau de la Grande-Terre, Nouvelle-Calédonie.
883   BRGM/RP-58531-FR. 114 p., 90 fig., 3 tabl., Bureau des Recherches Géologiques et Minières 2010.

884 Garcin, M., Gastaldi, Y., and Lesimple, S.: Quantification et évolution temporelle des apports miniers dans
885   les rivières calédoniennes. BRGM/RP-66840-FR, 44 p., 23 fig., 5, Bureau des Recherches Géologiques
886   et Minières

887 2017.

888 Gruszowski, K., Foster, I. D., Lees, J., and Charlesworth, S.: Sediment sources and transport pathways in a
889   rural catchment, Herefordshire, UK, Hydrological Processes, 17, 2665-2681, 2003.

890 Hedouin, L., Pringault, O., Metian, M., Bustamante, P., and Warnau, M.: Nickel bioaccumulation in bivalves
891   from the New Caledonia lagoon: Seawater and food exposure, Chemosphere, 66, 1449-1457, 2007.

892 Highley, D., Chapman, G. R., and Bonel, K.: The economic importance of minerals to the UK, British
893   Geological Survey, 2004.

894 Iltis, J.: La mine, élement de la controverse écologique dans le Pacifique Sud, L'Espace géographique, 193-
895   205, 1992.

896 James, L. A.: Legacy sediment: definitions and processes of episodically produced anthropogenic
897   sediment, Anthropocene, 2, 16-26, 2013.

898 Juillot, F.: – Rapport scientifique final. Programme « Dynamique des métaux de la mine au lagon ». CNRT
899   « Nickel & son environnement ». 202 pages., 2019.

900 Klages, M., and Hsieh, Y.: Suspended Solids Carried by the Gallatin River of Southwestern Montana: II.
901   Using Mineralogy for Inferring Sources 1, Journal of Environmental Quality, 4, 68-73, 1975.

902 Kumar, A., and Maiti, S. K.: Assessment of potentially toxic heavy metal contamination in agricultural
903   fields, sediment, and water from an abandoned chromite-asbestos mine waste of Roro hill, Chaibasa,
904   India, Environmental earth sciences, 74, 2617-2633, 2015.

905 Laceby, J. P., and Olley, J.: An examination of geochemical modelling approaches to tracing sediment
906   sources incorporating distribution mixing and elemental correlations, Hydrol. Process., 29, 1669-1685,
907   10.1002/hyp.10287, 2015.

908 Laceby, J. P., Evrard, O., Smith, H. G., Blake, W. H., Olley, J. M., Minella, J. P. G., and Owens, P. N.: The
909   challenges and opportunities of addressing particle size effects in sediment source fingerprinting: A
910   review, Earth-Sci. Rev., 169, 85-103, 10.1016/j.earscirev.2017.04.009, 2017.

911 Le Gall, M., Evrard, O., Foucher, A., Laceby, J. P., Salvador-Blanes, S., Manière, L., Lefèvre, I., Cerdan, O.,
912   and Ayrault, S.: Investigating the temporal dynamics of suspended sediment during flood events with
913   7 Be and 210 Pb xs measurements in a drained lowland catchment, Scientific reports, 7, 42099, 2017.

914 Legout, C., Poulenard, J., Nemery, J., Navratil, O., Grangeon, T., Evrard, O., and Esteves, M.: Quantifying
915   suspended sediment sources during runoff events in headwater catchments using spectrocolorimetry,
916   J Soils Sediments, 13, 1478-1492, 10.1007/s11368-013-0728-9, 2013.

917 Mardhel, V., Iseppi, M., Regninger, P. A., and Sevin, B.: Connaissance de l'ophiolite, géophysique
918   aéroportée et étude de la structure. Rapport scientifique final. Programme «OPHIOSTRUCT». CNRT
919   «Nickel & son environnement», 2018.

920 Martínez-Carreras, N., Udelhoven, T., Krein, A., Gallart, F., Iffly, J. F., Ziebel, J., Hoffmann, L., Pfister, L., and
921   Walling, D. E.: The use of sediment colour measured by diffuse reflectance spectrometry to determine
922   sediment sources: application to the Attert River catchment (Luxembourg), J Hydrol, 382, 49-63, 2010.

923 Motha, J., Wallbrink, P., Hairsine, P., and Grayson, R.: Unsealed roads as suspended sediment sources in
924   an agricultural catchment in south-eastern Australia, Journal of Hydrology, 286, 1-18, 2004.

925 Navratil, O., Evrard, O., Esteves, M., Legout, C., Ayrault, S., Némery, J., Mate-Marin, A., Ahmadi, M.,
926   Lefèvre, I., and Poirel, A.: Temporal variability of suspended sediment sources in an alpine catchment
927   combining river/rainfall monitoring and sediment fingerprinting, Earth Surface Processes and
928   Landforms, 37, 828-846, 2012.

929 Owens, P. N., and Walling, D. E.: The phosphorus content of fluvial sediment in rural and industrialized
930   river basins, Water Res., 36, 685-701, 2002.

931 Pascal, N.: Ecosystèmes coralliens de Nouvelle-Calédonie. Valeur économique des services
932   écosystémiques. Partie I: Valeur financière. IFRECOR., 2010.

933 Poulenard, J., Perrette, Y., Fanget, B., Quetin, P., Trevisan, D., and Dorioz, J.-M.: Infrared spectroscopy
934   tracing of sediment sources in a small rural watershed (French Alps), Science of the Total Environment,
935   407, 2808-2819, 2009.

936 Poulenard, J., Legout, C., Nemery, J., Bramorski, J., Navratil, O., Douchin, A., Fanget, B., Perrette, Y., Evrard,
937   O., and Esteves, M.: Tracing sediment sources during floods using Diffuse Reflectance Infrared Fourier
938   Transform Spectrometry (DRIFTS): A case study in a highly erosive mountainous catchment (Southern
939   French Alps), Journal of Hydrology, 414, 452-462, 2012.

940 Priadi, C., Ayrauk, S., Pacini, S., and Bonte, P.: Urbanization impact on metals mobility in riverine
941   suspended sediment: role of metal oxides, International Journal of Environmental Science &
942   Technology, 8, 1-18, 2011.

943 Prior, T., Daly, J., Mason, L., and Giurco, D.: Resourcing the future: Using foresight in resource governance,
944   Geoforum, 44, 316-328, 2013.

945 Quantin, P., Bourdon, E., and Becquer, T.: Minéralogie et contraintes édaphiques des sols" ferritiques"
946   dérivés de roches ultrabasiques en Nouvelle-Calédonie: relations entre constituants minéraux et
947   disponiblité en certains éléments (Al, Fe, Si, Mg, Mn, Ni, Co, Cr, Cu, Zn, Mo) facilement solubles, 1997.

948 Rossel, R. V., Walvoort, D., McBratney, A., Janik, L. J., and Skjemstad, J.: Visible, near infrared, mid infrared
949   or combined diffuse reflectance spectroscopy for simultaneous assessment of various soil properties,
950   Geoderma, 131, 59-75, 2006.

951 Sellier, V., Navratil, O., Laceby, J. P., Allenbach, M., Lefèvre, I., and Evrard, O.: Investigating the use of
952   fallout and geogenic radionuclides as potential tracing properties to quantify the sources of suspended
953   sediment in a mining catchment in New Caledonia, South Pacific, Journal of Soils and Sediments, 1-17,
954   2019.

955 Sevin, B.: Cartographie du régolithe sur formation ultrabasique de Nouvelle-Calédonie: Localisation dans
956   l'espace et le temps des gisements nickélifères, Nouvelle Calédonie, 2014.

957 Shellberg, J., Brooks, A., and Spencer, J.: Land-use change from indigenous management to cattle grazing
958   initiates the gullying of alluvial soils in northern Australia, 19th World Congress of Soil Science: Soil
959   Solutions for a Changing World, 2010, 1-6,

960 Sherriff, S. C., Franks, S. W., Rowan, J. S., Fenton, O., and Ó'hUallacháin, D.: Uncertainty-based assessment
961   of tracer selection, tracer non-conservativeness and multiple solutions in sediment fingerprinting using
962   synthetic and field data, J Soils Sediments, 15, 2101-2116, 10.1007/s11368-015-1123-5, 2015.

963 Smith, H. G., Sheridan, G. J., Lane, P. N. J., Noske, P. J., and Heijnis, H.: Changes to sediment sources
964   following wildfire in a forested upland catchment, southeastern Australia, Hydrol. Process., 25, 2878-
965   2889, 10.1002/hyp.8050, 2011.

966 Surell, A.: Étude sur les torrents des Hautes-Alpes, Carilian-Goeury, 1841.

967 Tiecher, T., Caner, L., Minella, J. P., and dos Santos, D. R.: Combining visible-based-color parameters and
968   geochemical tracers to improve sediment source discrimination and apportionment, Sci Total Environ,
969   527-528, 135-149, 10.1016/j.scitotenv.2015.04.103, 2015.

970 Trescases, J. J.: Weathering and geochemical behaviour of the elements of ultramafic rocks in New
971   Caledonia, BMRJ. Aust. Geol and Geophys., 141, 149-161, 1973.

972 Uber, M., Legout, C., Nord, G., Crouzet, C., Demory, F., and Poulenard, J.: Comparing alternative tracing
973   measurements and mixing models to fingerprint suspended sediment sources in a mesoscale
974   Mediterranean catchment, Journal of Soils and Sediments, 1-19, 2019.

975 Valette-Silver, N. J.: The use of sediment cores to reconstruct historical trends in contamination of
976   estuarine and coastal sediments, Estuaries, 16, 577-588, 1993.

977 Varol, M.: Assessment of heavy metal contamination in sediments of the Tigris River (Turkey) using
978   pollution indices and multivariate statistical techniques, Journal of Hazardous Materials, 195, 355-364,
979   2011.

980 Wallbrink, P., Murray, A., Olley, J., and Olive, L.: Determining sources and transit times of suspended
981   sediment in the Murrumbidgee River, New South Wales, Australia, using fallout 137Cs and 210Pb,
982   Water Resour Res, 34, 879-887, 1998.

983 Wallbrink, P. J.: Quantifying the erosion processes and land-uses which dominate fine sediment supply to
984   Moreton Bay, Southeast Queensland, Australia, Journal of environmental radioactivity, 76, 67-80,
985   2004.

986 Walling, D., Peart, M., Oldfield, F., and Thompson, R.: Suspended sediment sources identified by magnetic
987   measurements, Nature, 281, 110, 1979.

988 Yellishetty, M., Mudd, G. M., and Shukla, R.: Prediction of soil erosion from waste dumps of opencast
989   mines and evaluation of their impacts on the environment, International Journal of Mining,
990   Reclamation and Environment, 27, 88-102, 2013.

991